

1 **Global evaluation of ELMv1-CNP and the role of the phosphorus cycle in the historical**
2 **terrestrial carbon balance**

3
4 Xiaojuan Yang^{1*}, Peter Thornton¹, Daniel Ricciuto¹, Yilong Wang^{2,3}, Forrest Hoffman⁴

5 ¹Environmental Sciences Division, Oak Ridge National Lab, Oak Ridge, TN 37831, USA

6 ²Key Laboratory of Land Surface Pattern and Simulation, Institute of Geographic
7 Sciences and Natural Resources Research, Chinese Academy of Sciences, Beijing, China

8 ³Laboratoire des Sciences du Climat et de l'Environnement, CEA-CNRS-UVSQ- Université
9 Paris Saclay, 91191, Gif-sur-Yvette CEDEX, France

10 ⁴Computational Sciences & Engineering Division, Oak Ridge National Lab, Oak Ridge, TN
11 37831, USA

12
13
14
15
16
17 ****Corresponding Author:***

18 **Phone:** 865-5747615

19 **E-mail:** yangx2@ornl.gov

38 **Abstract**

39 The importance of carbon (C)-nutrient interactions to the prediction of future C uptake has long
40 been recognized. The Energy Exascale Earth System Model (E3SM) land model (ELM) version 1
41 is one of the few land surface models that include both N and P cycling and limitation (ELMv1-
42 CNP). Here we provide a global scale evaluation of ELMv1-CNP using International Land Model
43 Benchmarking (ILAMB) system. We show that ELMv1-CNP produces realistic estimates of
44 present-day carbon pools and fluxes. Compared to simulations with optimal P availability,
45 simulations with ELMv1-CNP produces better performance, particularly for simulated biomass,
46 leaf area index (LAI), and global net C balance. We also show ELMv1-CNP simulated N and P
47 cycling are in good agreement with data-driven estimates. We compared ELMv1-CNP simulated
48 response to CO₂ enrichment with meta-analysis of observations from similar manipulation
49 experiments. We show that ELMv1-CNP is able to capture the field observed responses for
50 photosynthesis, growth, and LAI. We investigated the role of P limitation in the historical
51 balance and show that global C sources and sinks are significantly affected by P limitation, as
52 the historical CO₂ fertilization effect was reduced by 20% and C emission due to land use and
53 land cover change was 11% lower when P limitation was considered. Our simulations suggest
54 that introduction of P cycle dynamics and C-N-P coupling will likely have substantial
55 consequences for projections of future C uptake.

56

57

58

59

60

61

62

63

64

65

66

67 Copyright statement:

68
69 *This manuscript has been authored by UT-Battelle, LLC under Contract No. DE-AC05-00OR22725 with the*
70 *US Department of Energy. The United States Government retains and the publisher, by accepting the*
71 *article for publication, acknowledges that the United States Government retains a non-exclusive, paid-*
72 *up, irrevocable, world-wide license to publish or reproduce the published form of this manuscript, or*
73 *allow others to do so, for United States Government purposes. The Department of Energy will provide*
74 *public access to these results of federally sponsored research in accordance with the DOE Public Access*
75 *Plan (<http://energy.gov/downloads/doe-public-access-plan>).*

76
77
78
79
80
81
82
83
84
85
86
87
88
89
90
91
92
93
94
95
96
97
98
99

100 1. Introduction

101 The recent global carbon (C) budget showed that over the last half century global
102 fossil CO₂ emissions have increased from about 3 Pg C/yr in 1960s to about 9.5 PgC/yr in the
103 last decade (Friedlingstein et al., 2019). It has also been shown that land ecosystems play
104 important roles in controlling the fractions of CO₂ emissions that remain in the atmosphere
105 by taking up about 29% of total emissions (Le Quéré et al., 2018). Large uncertainties
106 remain on the net land-atmosphere C exchange, mainly due to difficulties in quantifying the
107 complex C cycle processes such as CO₂ fertilization effects, responses of carbon fluxes to
108 temperature and precipitation variation, and C emissions associated with land use and land
109 cover change (LULCC). These uncertainties will very likely hamper our ability to predict the
110 future trajectories of atmospheric CO₂.

111 One of the important uncertainties relates to our understanding of C-nutrient
112 interactions and nutrient limitation and how they are represented in models. The
113 importance of nitrogen (N) availability to predicted land C storage has been long recognized
114 (Hungate et al., 2003). Although there were only two models in CMIP5 (the fifth phase of
115 the Coupled Model Intercomparison Project) that accounted for N dynamics and N
116 limitation (Thornton et al., 2007; Thornton et al., 2009; Arora et al., 2013), many ESMs
117 participating in CMIP6 (the Coupled Model Intercomparison Project phase 6) are now
118 including N cycle and C-N interactions (Davies-Barnard et al., 2020; Lawrence et al., 2019;
119 Goll et al., 2017a; Smith et al., 2014; Sellar et al., 2019). The comparisons between these
120 models have been summarized in Arora et al. (2020) and Davies-Barnard et al. (2020). In
121 recent years, significant efforts have also gone into understanding phosphorus (P) cycle
122 dynamics and the role of P limitation in land C storage (Jiang et al., 2019; Hou et al., 2020;
123 Reed et al., 2015; Wieder et al., 2015b; Sun et al., 2017). Increasing numbers of models
124 have developed the capability to include P cycle processes and C-N-P interactions (Wang et
125 al., 2010; Goll et al., 2012; Thum et al., 2019; Goll et al., 2017b; Yang et al., 2014; Yang et al.,
126 2019; Sun et al., 2021). It has been shown that considering P cycle dynamics and C-N-P
127 interactions improves process representation and model fidelity compared with
128 observational and experimental data in most models (Goll et al., 2017b; Yang et al., 2014).

129 Model simulations have also demonstrated the importance of P limitation to land C uptake
130 (Zhang et al., 2014; Goll et al., 2012; Yang et al., 2016; Yang et al., 2019; Sun et al., 2021).
131 Using an ensemble of 14 terrestrial ecosystem models to simulate the planned free-air CO₂
132 enrichment experiment AmazonFACE, Fleischer et al. (2019) showed that P availability
133 reduced the projected CO₂-induced C sink by about 50% compared to estimates from
134 models assuming no phosphorus limitation. Taken together, understanding and
135 representation of the role of P cycle dynamics in affecting terrestrial C balance is essential
136 for the prediction of future terrestrial carbon uptake and atmospheric CO₂ concentration.

137 Field and modeling studies have shown that forest productivity tends to increase with
138 increasing soil phosphorus availability (Vicca et al., 2012; Aragão et al., 2009; Wang et al.,
139 2010). Despite these recent efforts, P cycle dynamics and C-N-P interactions are not yet
140 included in most CMIP6 models. The Energy Exascale Earth System Model(E3SM) is one of
141 the few models that have been developed a coupled C-N-P capability in the land component
142 in CMIP6 (Burrows et al., 2020). The land model in E3SM, herein referred to as ELMv1-CNP,
143 has been first applied in the Amazon region to test its capability and to evaluate the
144 importance of P limitation in this region (Yang et al., 2019). Yang et al. (2019) provides an in-
145 depth evaluation of ELMv1-CNP for the Amazon rainforest using field observational data,
146 with a focus on how the introduction of P cycle dynamics and P limitation improved model
147 simulated spatial variation of productivity. They show that effects of P limitation on C
148 sources and sinks in the Amazon region are significant, reducing simulated CO₂ fertilization
149 of new carbon uptake by as much as 31%.

150 This study expands the analysis in the Amazon region to the global scale and has two
151 main aims: (1) to provide an evaluation of ELMv1-CNP performance on the global scale
152 using both observational and experimental data, and (2) to quantify the role of P cycle
153 dynamics and P limitation in affecting simulated C sources and sinks globally. We first
154 evaluate the performance of ELMv1-CNP using the ILAMB benchmarking system (Collier et
155 al., 2018), which has been widely used in the evaluation of land surface models and ESMs
156 (Lawrence et al., 2019; Bonan et al., 2019; Zhu et al., 2019; Friedlingstein et al., 2019). We
157 then evaluate ELMv1-CNP simulated N and P pools and fluxes with an observation-based

158 dataset. Realizing that the static benchmarking may not help constrain future model
159 projections, we further evaluate ELMv1-CNP using experimental manipulations of
160 atmospheric CO₂. Finally, we take advantage of the P-enabled capability in ELMv1-CNP to
161 quantify the effect of P dynamics on the simulated ecosystem responses to increasing
162 atmospheric CO₂, increasing N deposition, LULCC, and climate change on the global scale.

163

164 **2. Method**

165 **2.1 Model Overview**

166 ELMv1-CNP is based on the Community Land Model version 4.5 (CLM4.5), which
167 includes coupled C-N biogeochemistry from CLM4 (Thornton et al., 2007) and
168 improvements to canopy photosynthesis, soil biogeochemistry and representation of
169 nitrogen cycle dynamics (Koven et al., 2013; Bonan et al., 2011; Oleson et al., 2013).
170 Recognizing the critical role of the tropical forests in the global carbon cycle and C-climate
171 interactions and the important role of P cycle dynamics and P limitation in tropical forests,
172 we implemented a fully prognostic P cycle and C-N-P interactions into ELMv1-CNP, enabling
173 ELMv1-CNP to be one of the few land surface models that include both N and P cycle
174 dynamics and limitation. The main model features include (1) a fully prognostic P cycle
175 tracking various soil inorganic P pools, vegetation P pools, litter and soil organic P pools (2)
176 the representation of P limitation on plant productivity and litter and soil organic matter
177 decomposition based on a supply-demand approach (3) resolving N vs P limitation using
178 the Liebig law (4) the vertically-resolved soil inorganic and organic P dynamics (5) the
179 decoupling of P cycle from C and N cycle during decomposition due to phosphatase activity
180 (6) the representation of adsorption-desorption dynamics based on soil order.

181 Besides the P cycling processes, the other important difference of ELMv1-CNP from
182 CLM4.5 is the removal of instantaneous downregulation of photosynthesis from nutrient
183 limitation. Instead, longer-term downregulation of productivity is enabled through the
184 implementation of C, N, and P nonstructural vegetation storage pools. In CLM4.5, nutrient
185 limitation is calculated at each time step as a function of potential GPP, stoichiometry of
186 plant tissues, and nitrogen uptake. Any “excess” carbon due to nitrogen limitation is

187 immediately released to the atmosphere through instantaneous downregulation. This
188 nutrient limitation can be highly variable over time and affects diurnal and seasonal cycles
189 of gross primary productivity, which is not consistent with flux tower observations (Ghimire
190 et al., 2016) or with short-term elevated CO₂ experiments that were done with and without
191 nutrient fertilization (Metcalf et al., 2017). In the current model, competition for available
192 nutrients and plant uptake still occur every timestep given instantaneous demand that is a
193 function of plant GPP and microbial nutrient immobilization (Oleson et al.,
194 2013). However, nutrients taken up by plants are now first allocated to non-structural N
195 and P storage pools instead of directly to structural pools. Nutrient limitation to allocation
196 is determined by comparing plant nutrient demand (given GPP and stoichiometry) and the
197 nutrient availability from the non-structural nutrient pools, which is a function of the pool
198 size in relation to long-term demand. The “excess” carbon flux, which cannot be allocated
199 due to nutrient limitation, is directed to the non-structural plant carbon (NSC) pool instead
200 of downregulating GPP. This pool respire to the atmosphere with a given turnover time.
201 Details about the representation of NSC can be found in the supporting information (Text
202 S1)

203 The model version used in this study is the publicly released ELM v1 and can be
204 downloaded along with all the parameter files at <https://github.com/E3SM-Project/E3SM>.
205 In this version of the model, the fire module is activated by default. The soil erosion module
206 is not activated. We assume soil C, N, and P cycling can take place to the 3.8m depth as the
207 assumption in CLM4.5 (Koven et al., 2013). We also provide the key model parameters in
208 Table S1 (PFT specific) and Table S2 (soil order specific). We note that only leaf parameters
209 vary with PFT, but we include all other tissues in Table S1 to provide all parameters in the
210 consistent format.

211

212 **2.2 Simulations**

213 The simulations presented here were first spun up to bring C, N, and P pools to
214 equilibrium by recycling the GSWP3 (Global Soil Wetness Project Phase 3) climate forcing
215 data (<http://hydro.iis.u-tokyo.ac.jp/GSWP3/>) between 1901-1920, along with constant

216 atmospheric CO₂, N deposition and land cover type at year 1850. Spinup was accomplished
217 through two steps: accelerated decomposition (AD) spinup and regular spinup. We ran the
218 model for 250 years in the AD spinup mode. The purpose of the AD spinup is to accelerate
219 the decomposition process and speed up the spinup process of the carbon and nutrient
220 cycles. The AD spinup procedure was modified from that originally described by Thornton
221 and Rosenbloom (2005), which used spatially invariant acceleration factors to accelerate
222 decomposition in soil organic matter (SOM) pools. Here we updated the AD spinup by
223 including the impacts of temperature and soil moisture on the acceleration factor. This
224 resulted in higher acceleration factors in cool and/or dry climates, which are typically slower
225 to achieve steady state. In addition, vegetation dead stem and coarse root mortality
226 were accelerated by a factor of 10 to achieve steady state biomass more quickly. The factor
227 of 10 was chosen to have a good balance between faster acceleration and the
228 disequilibrium between accelerated and non-accelerated steady states that requires a
229 longer regular spinup following Koven et al. (2013). In the AD spinup, supplemental soil
230 mineral P was applied for the entire simulation such that there was no P limitation on C and
231 N dynamics. During the transition between AD spinup and regular spinup, we initialized the
232 soil inorganic pools using global P maps developed by (Yang et al., 2013). For the grid cells
233 that don't have values in Yang et al. (2013), we applied the nearest neighbor method to
234 estimate the values. Since the P cycle involves both biological and geochemical processes
235 that occur on geological time scales, the initialization of P pools provides some reasonable
236 estimates of soil P pools without running the model for millions of simulated years. More
237 details regarding the rationale of using the developed P maps for initialization can be found
238 in Yang et al. (2013). We then ran normal spinup for 600 years with active C, N, and P
239 coupled biogeochemistry until C, N, and P pools reached equilibrium. The criteria for
240 equilibrium are for global total NEE less than 0.1 PgC/yr averaged over 100 years, the
241 threshold recommended for the C4MIP (Jones et al., 2016). We also ran a control simulation
242 between 1850-2010 as a continuation of the normal spinup. We added the time series of
243 labile P, secondary mineral P and occluded P for the control simulation (Fig. S1). There are
244 very little changes in the inorganic P pools during the 161 years control simulation

245 suggesting that these pools can be considered in equilibrium for the time scale of our
246 interest.

247 After the model was spun up, we ran the global historical transient simulations (1850–
248 2010) at 0.5 degree spatial resolution using GSWP3 v2 climate forcing data, along with
249 historical transient atmospheric CO₂ concentration, N deposition, land use and land cover
250 change that are part of the CMIP6 protocols (<https://luh.umd.edu/data.shtml>). Input data
251 and references are summarized in Table S3. We also ran a suite of single-factor simulations
252 to examine the individual effects of changing environmental factors (atmospheric CO₂, land
253 use and land cover change, climate, and nitrogen deposition, Table 1). In addition to the
254 ELM v1 simulations with a fully active P cycle, we also performed historical transient and
255 single-factor simulations with P limitation switched off (supplementing P availability to fully
256 meet demand at each grid cell and for each timestep so there is no P limitation on
257 productivity and decomposition). We denoted the default ELM v1 simulations that have an
258 active P cycle as the CNP configuration (ELMv1-CNP) and simulations assuming no P
259 limitation as the CN configuration (ELMv1-CN).

260 We also performed one additional simulation where we initiated a global step increase
261 of atmospheric CO₂ concentration, by +200ppm, starting from 2001 and continuing through
262 2010. These simulations are designed to mimic the Free Air CO₂ Enrichment (FACE)
263 experiments (Ainsworth and Long, 2005). To quantify model sensitivities to elevated CO₂,
264 we calculated the effect size (treatment divided by control) over the 10 years of simulation
265 (2001-2010). We then evaluated model sensitivities to elevated CO₂ against meta-analysis
266 from FACE experiments (Ainsworth and Long 2005).

267 All of the simulations are summarized in Table 1.

268

269 **2.3. ILAMB**

270 We used the International Land Model Benchmarking system (Collier et al., 2018; Luo et
271 al., 2012; Hoffman et al., 2017) to assess the model performance. ILAMB was designed to
272 use a wide array of observational data to constrain model results, including various land
273 carbon pools and fluxes, inferred CO₂ concentration variability, and functional relationships.

274 For each variable, ILAMB scores model performance for period mean, bias, root-mean-
275 square error (RMSE), spatial distribution, interannual coefficient of variation, seasonal cycle,
276 and long-term trend. These scores are aggregated into an overall score representing
277 multiple aspects of model performance for each variable. These aggregated absolute scores
278 are then used to calculate the relative score, which indicates the relative performance of
279 each model with respect to other models used in the same analysis. The observational
280 datasets used for the evaluation of carbon cycle in ILAMB are listed in Table S4.

281 In order to understand how the implementation of P cycling dynamics affects model
282 performance, we evaluated the performance of both ELMv1-CNP and ELMv1-CN. In order to
283 provide a context in terms of model performance in ILAMB, we provide the ILAMB
284 evaluation of several other land models included in the Land Surface, Snow and Soil
285 moisture Model Intercomparison Project (LS3MIP) as part of CMIP6 ([https://www.wcrp-
286 climate.org/wgcm-cmip/wgcm-cmip6](https://www.wcrp-climate.org/wgcm-cmip/wgcm-cmip6)). LS3MIP includes a collection of model experiments
287 including both offline land model experiments and coupled experiments (Van Den Hurk et
288 al., 2016). We used the results from the offline land model experiments. Like our
289 simulations, these experiments were performed at 0.5by0.5 spatial resolution and using the
290 GSWP3 forcing data. Other model configurations in LS3MIP are identical to that used in
291 CMIP6 historical simulations, which we used for the simulations in this study.

292

293 2.4. GOLUM-CNP

294 Since there is no nutrient cycle metrics in ILAMB, we also compared major N and P pools
295 and fluxes along with nutrient use efficiencies from ELMv1-CNP with the data-driven
296 estimates of N and P pools and fluxes from the Global Observation-based Land-ecosystems
297 Utilization Model of Carbon, Nitrogen, and Phosphorus (GOLUM-CNP) (Wang et al., 2018).
298 GOLUM-CNP combines data-driven estimates of N and P inputs and outputs and observed
299 stoichiometric ratios with a steady-state diagnostic model, providing global steady-state N
300 and P pools and fluxes for large biomes. Despite large uncertainties and the steady-state
301 assumptions, GOLUM-CNP provides a global data-driven product that can be used to test

302 nutrient cycles in land surface models. GOLUM-CNP has also been used in the evaluation of
303 other land surface models (Sun et al., 2021).

304

305 **3. Results**

306 **3.1 Evaluations of ELM v1 using ILAMB**

307 ILAMB includes many metrics that cover water, energy, and carbon pools and fluxes on
308 both regional and global scales. Fig. 1 shows ILAMB benchmarking scores for ELMv1-CNP
309 and ELMv1-CN, along with several other land models in CMIP6, which are provided to
310 contextualize ILAMB scores for ELMv1-CNP. The relative model performance scores are
311 shown in Fig. 1, indicating which model version performs better with respect to others. The
312 full results produced by the ILAMB package can be found at [https://compy-
313 dtn.pnl.gov/yang954/build/](https://compy-dtn.pnl.gov/yang954/build/).

314 Fig. 1 shows that the performance of ELMv1-CNP is comparable to other land models in
315 CMIP6. ELMv1-CNP exhibits performance similar to CLM5 (CESM2) in terms of aggregated
316 scores for carbon cycle metrics, while CLM5 shows better performance with respect to
317 overall functional relationships, mainly due to a better score for functional relationship of
318 burned area. The performance of each model varies for different variables. For example,
319 ORCHIDEE land surface model in IPSL-CM6A-LR performs relatively well in inferred
320 atmospheric carbon dioxide, leaf area index and GPP relationships.

321 Fig.1 also shows the comparison between ELM v1-CNP and ELM v1-CN, allowing us to
322 quantify the impacts of including a prognostic P cycle and realistic P availability on model
323 performance. For metrics in Fig. 1 that show the greatest differences between ELMv1-CNP
324 and ELMv1-CN, the CNP version always has a higher score than CN. This is reflected in the
325 relatively higher aggregated scores for carbon cycle variables and functional relationships
326 in ELMv1 -CNP.

327

328 Fig. 2 shows the Global Net Ecosystem Carbon Balance metric in ILAMB for ELM v1-CNP
329 and ELM v1-CN. The observational data sets for this metric are from the Global Carbon
330 Project (Fig. 2a)(Le Quéré et al., 2016) and from the inversion-based estimate (Hoffman et

331 al., 2014), both providing global totals of land carbon accumulation but for different
332 historical time period (1850-2010 for Hoffman et al., 2014 and 1959-2010 for Le Quere et l.,
333 2016). The simulated global C balance by both ELMv1-CNP and ELMv1-CN are in the range
334 of uncertainty of observational estimates, with ELMv1-CNP simulated historical global
335 carbon accumulation being a better match with mean observational estimates, particularly
336 after 1950. ELMv1-CN estimated a net accumulation of land carbon of 22 Pg C over the
337 period 1850-2010, which is much higher than the mean observational estimate of - 8Pg C.
338 ELMv1-CNP estimated land carbon accumulation of 7 Pg C.

339 Fig. 3 shows the spatial distribution of vegetation biomass for the benchmark data and
340 model bias in ILAMB. Overall both ELMv1-CN and ELMv1-CNP tend to overestimate
341 biomass, compared to this specific global product of biomass (GEOCARBON). The high bias
342 in the tropical region is much reduced in ELMv1-CNP simulations (Fig. 3a, 3b and 3c). The
343 better performance of ELMv1-CNP is also reflected in the spatial Taylor diagram for
344 biomass (Fig. 3d).

345 Another important benchmark in ILAMB is the functional relationships between two
346 variables, for example the relationship between GPP and precipitation and the relationship
347 between annual mean LAI and precipitation. An accurate simulation of these relationships
348 in addition to individual benchmarks is an indication that the models are representing the
349 underlying processes correctly. ELMv1-CNP produces a better functional relationship
350 compared to ELMv1-CN. For example, for the relationship between LAI and precipitation
351 ELMv1-CN overestimated LAI, particularly in regions with high precipitation, while the
352 ELMv1-CNP configuration shows an improved relationship (Fig. 4). The improvement of the
353 functional relationship is mainly due to the improvement in high precipitation regions, e.g.
354 lowland tropical forest regions. In these regions, inclusion of P dynamics and P limitation
355 reduced simulated bias in GPP and LAI, therefore leading to better match with the
356 observations.

357

358 3.2. Evaluation of N and P cycling in ELMv1-CNP

359 We evaluated simulated nutrient use efficiencies against that from GOLUM-CNP product
360 on the biome level. Here we define nutrient use efficiency as the ratio between annual NPP
361 and annual nutrient uptake (for both N and P), with NUE for nitrogen use efficiency and
362 PUE for phosphorus use efficiency (Finzi et al., 2007). ELMv1-CNP simulated NUE is higher
363 in temperate and boreal forests and lower in tropical grassland and tundra, which is
364 consistent with GOLUM-CNP (Fig. 5a). [Temperate grassland NUE and PUE in ELMv1-CNP are
365 higher in distribution because of the higher variation in NPP allocation to non-structural
366 carbon pools.](#) ELMv1-CNP predicted higher NUE in tropical lowland forests than GOLUM-
367 CNP. ELMv1-CNP simulated PUE is generally consistent with GOLUM -CNP (Fig. 5b).
368 However, ELMv1-CNP simulated PUE in tropical forests is much lower than that from
369 GOLUM-CNP.

370 We also evaluated ELMv1-CNP simulated N and P pools and major fluxes on the global
371 scale for the period of 2001-2010 with the observationally derived products in GOLUM-
372 CNP. Fig. S2 shows the comparison of N and P uptake from ELMv1-CNP and GOLUM-CNP at
373 the biome level. ELMv1-CNP simulated plant N and P uptake is in agreement with GOLUM-
374 CNP, with higher uptake fluxes in tropical forests and lower uptake in temperate and boreal
375 forests. ELMv1-CNP simulated N uptake is lower in the tropical forests, compared to
376 GOLUM-CNP (Fig. S2a). Conversely, simulated P uptake is higher than GOLUM-CNP
377 estimates across the tropics (Fig. S2b).

378

379 **3.2 Evaluations using CO₂ manipulation experiment**

380 Relative to the control simulation, increasing atmospheric CO₂ concentration by 200ppm
381 increased gross primary productivity by 23% (global mean) over the 10 years of simulation
382 (2001-2010). Nearly all PFTs showed more than a 10% increase in productivity, with more
383 significant increases occurring in tropical regions and middle latitudes (Fig. 6a). The
384 modeled response ratio of NPP is also showing widespread increases, and on the global
385 scale our results showed a 25.8% increase in NPP in response to CO₂ enrichment (Fig. 6b).
386 The simulated increases in GPP and NPP also showed, to a large extent, translated into
387 increases in vegetation carbon (Fig 6c), with a global average response ratio of 18%. The

388 modeled response ratio of LAI is much smaller, a 5% increase globally (Fig 6d). The globally
389 aggregated simulated effect size of CO₂ enrichment from ELMv1-CNP on GPP, NPP, LAI and
390 NSC compare well to the observations from the meta-analysis (Fig. 7), particularly for GPP
391 and LAI. ELMv1-CNP overestimated the responses of NPP. Both observations and
392 simulations show large sensitivity of NSC to CO₂ enrichment, with larger variability in the
393 model simulations.

394

395 **3.3. Carbon, nitrogen and phosphorus pools and fluxes**

396 **3.3.1 Carbon budget**

397 Major components of the global land C budget for present day (mean of 2001–2010) in
398 ELMv1-CNP are shown in Fig 8a. These are from historical simulations with transient climate
399 forcing, atmospheric CO₂ concentration, land use and land cover change, and N deposition.
400 For the present day, model simulated total ecosystem C is 2588.73 Pg C, with about 22%
401 stored in vegetation (575.45 Pg C), about 5% stored in litter and coarse wood debris (122.5
402 Pg C), and 73% stored in soil organic matter (1890.78 Pg C). Model simulated vegetation C is
403 within the range of inventory-based estimates from IPCC AR5 (450–650 Pg C). Our simulated
404 vegetation C is also comparable to or slightly higher than observational estimates from the
405 literature: 455Pg C (GEOCARBON, (Avitabile et al., 2016; Santoro et al., 2015), 550±100 Pg C
406 (Houghton, 2003), 560±94 Pg C (Defries et al., 1999), and 450 Pg C (Erb et al., 2018). Model
407 simulated total soil C is within the range of estimates from IPCC AR5 (1500-2400 Pg C) and
408 that from Jobbágy and Jackson (2000) (1750±250 PgC). Model simulated total soil C is lower
409 than several other observational estimates from the literature: 2376-2456 (Batjes, 2014),
410 3000 Pg C (Köchy et al., 2015), which could be because ELMv1-CNP has yet to include an
411 explicit representation of peatland carbon dynamics. As for the top 1m soil carbon, model
412 simulated values of 1134.41 Pg C are within the range of estimates from the Harmonized
413 World Soil Database (HWSD) (FAO/IIASA/ISRIC/ISSCAS/JRC, 2012) as reported by Todd-
414 Brown et al. (2013) (890-1660 Pg C), but lower than the observational based estimate of
415 1462–1548 Pg C from Batjes (2014) and 1325 Pg C from Köchy et al. (2015). Model
416 simulated litter C (22.9 Pg C) is lower than the observational based estimate: 68 Pg C

417 (Matthews, 1997) and 43 ± 3 Pg C (Pan et al., 2011). Model simulated coarse wood debris C
418 stock (99.6 Pg C) is higher than the observational based estimate: 75 Pg C (Matthews, 1997)
419 and 73 ± 6 Pg C (Pan et al., 2011).

420 Model simulated present day GPP(134.15 Pg C/yr) is slightly higher than observational
421 based estimate: 123 ± 8 Pg C/yr (Beer et al., 2010), 119 ± 6 Pg C/yr (Jung et al., 2011) and 123
422 PgC/yr (IPCC AR5), and lower than 150-175 Pg C/yr from Welp et al. (2011) that is derived
423 based on oxygen isotopes of atmospheric CO₂. A recent study based on satellite data
424 suggested a global GPP of 140 Pg C/yr for year 2007 (Joiner et al., 2018). The comparisons
425 between simulated carbon pools and fluxes and available observations are also included in
426 Table 2.

427

428 **3.3.2. Nitrogen budget**

429 The ELMv1-CNP estimated N budget for the present day (2001–2010) is summarized in
430 Fig 8b. Compared to the C cycle, there are fewer observational estimates for N pools and
431 fluxes. Most of the literature values are from other model simulations. Although not
432 appropriate for direct model evaluation, these modeling estimates from the literature
433 provide a broad context for us to evaluate our simulated pools and fluxes.

434 Model simulated vegetation N is 4.36 Pg N, which is comparable to the estimates from
435 some other modeling studies: 3.8 Pg N (Zaehle et al., 2010), 5.3 Pg N (Xu and Prentice,
436 2008) and lower than the estimates of 16 Pg N(Lin et al., 2000) and 18 Pg N (Yang et al.,
437 2009). Model simulated total soil organic matter N is 188.79 Pg N, which is reasonable
438 considering the observational based estimate for 1m of 95 Pg N (Post et al., 1985) and 133–
439 140 Pg N (Batjes, 2014). ELMv1-CNP estimated biological nitrogen fixation (BNF) of 89
440 TgN/yr is within the range of estimates from literature. Vitousek et al. (2013) estimated that
441 global BNF ranges between 40–100 TgN/yr using a mass-balance approach. A meta-analysis
442 by Davies-Barnard and Friedlingstein (2020) suggested that global inputs of BNF in natural
443 ecosystems range between 52 and 130 TgN/yr, with a median global value of 88 TgN/yr. For
444 the purpose of comparison, BNF estimates from CLM5 is 96.4 TgN/yr, slightly higher than

445 our estimate. The comparisons between simulated N pools and fluxes and available
446 observations are also included in Table 2.

447

448

449 **3.3.3 Phosphorus budget**

450

451 The ELMv1-CNP estimated P budget for the present day (2001–2010) is summarized in
452 Fig 8c. Very few observational data are available for P on the global scale. The only
453 observation-based global product is the global P maps developed by (Yang et al., 2013).
454 Model simulated vegetation P is 0.36 Pg P, which is comparable to the estimates from other
455 modeling studies ranging from 0.23 to 3 Pg P (Goll et al., 2012; Wang et al., 2010; Jahnke,
456 1992). Model simulated soil organic P is 3.75 Pg P, which is slightly lower than previous
457 studies 5.74 Pg P (Goll et al., 2012), 5-10 Pg P (Smil, 2000), and 8.6 Pg (Yang et al., 2013).
458 Model simulated soil mineral P for the top 40cm and 60cm is 63.24 Pg P and 81.32 Pg P
459 respectively, which are generally comparable to the estimate of 45 Pg P for top 50cm soil
460 from Yang et al. (2013). The comparisons between simulated P pools and fluxes and
461 available observations are also included in Table 2.

462

463 **3.4. The effects of P limitation on historical carbon cycle**

464 ELMv1-CNP calculates the extent of both N and P limitation for plant growth on the
465 global scale (Figs. 9a and 9b). Generally speaking, P is a more limiting nutrient in tropical
466 evergreen forests and savannas in South America and Africa, while N is more limiting in
467 temperate regions (Fig. 9a). The ratio between the P limitation factor and N limitation
468 factor illustrates the degree of N-P colimitation (Fig. 9b). N and P are co-limiting
469 productivity in tundra, boreal forests, and deserts.

470 Fig. 10 shows the simulated spatial patterns of productivity and carbon storage and
471 how they are affected by P dynamics and limitation. P dynamics strongly control land
472 carbon uptake and storage, particularly in tropical regions. Globally NPP is highest in
473 tropical evergreen forests and lower in middle to high latitude regions. Plant growth in
474 tropical regions, however, is generally limited by P availability, particularly in the central

475 and eastern Amazon basin and tropical Africa. The reduced productivity due to P limitation
476 translates into reduced vegetation carbon storage and soil carbon storage, with the
477 exception of tropical savannas, where fire dynamics also play an important role in
478 vegetation and soil carbon storage.

479
480 Fig. 11 shows the effects of P dynamics on historical global land carbon
481 accumulation. The introduction of P dynamics leads to a 19.5% reduction in global C
482 storage due to CO₂ fertilization between 1850 and 2010. The consideration of P dynamics
483 also leads to a lower estimate of land use emissions on the global scale(143.89 PgC vs
484 161.21 PgC) as CNP simulations generally show lower initial vegetation biomass. Increasing
485 N deposition generally leads to a small carbon accumulation between 1850 and 2010 in
486 both CN and CNP simulations globally. With P limitation, however, the global carbon
487 accumulation from N deposition is reduced by about a third. Climate, although responsible
488 for the large seasonal and interannual variability of carbon fluxes, has only minor impacts
489 on historical carbon accumulation on the global scale for both CN and CNP simulations.
490 When changes of all environmental factors are considered, the impact of P dynamics on
491 carbon accumulation is the balance between a smaller CO₂ fertilization effect and lower
492 land use emissions, with the net effect being slightly lower historical carbon accumulation
493 globally.

494

495 **4. Discussions**

496 **4.1. ILAMB benchmarking**

497 This study presents a global assessment of the ELMv1-CNP. Yang et al. (2019) evaluated
498 the performance of ELMv1-CNP in the Amazon region using plot-level observations from the
499 RAINFOR network and found that the model captures well the observed productivity and
500 biomass gradient across the Amazon basin. Here we further evaluate the global model
501 performance using the ILAMB benchmarking system – an open source land model
502 evaluation system that is designed to assess model performance at site level, regional, and
503 global scales in an integrated and comprehensive way.

504 We include several other land models in CMIP6 in our ILAMB analysis with the goal of
505 providing a context for the performance of ELMv1-CNP. We found that ELMv1-CNP exhibits
506 similar performance to other models. It is challenging to demonstrate a clear improvement
507 or degradation for complex land surface models in ILAMB. For example, our analysis
508 indicates that ELMv1-CNP performance is comparable to CLM5 in terms of the overall
509 carbon cycle. Both ELMv1-CNP and CLM5 have a common ancestor CLM4.5, but they took
510 very different approaches for further development. CLM5 had significant efforts undertaken
511 in improving the representation of nitrogen cycle, while ELMv1-CNP was more focused on
512 implementing a prognostic phosphorus cycle and C-N-P interactions. Model development
513 activities in both models helped improved model performance through the lens of ILAMB
514 but the sources of improvements are quite different. This highlights the need to include
515 more process-level evaluations in ILAMB for the purpose of evaluating the impact of specific
516 model improvements.

517 Although CLM5 and ELM-CNP perform similarly in terms of ILAMB scores, it is worth
518 noting the unique role of P cycle dynamics in affecting C cycling and the importance of
519 including P cycle limitation in earth system models for better prediction of carbon-climate
520 feedbacks. The important role of soil P availability in affecting plant growth in tropical
521 forests residing on highly weathered soils has long been recognized (Walker and Syers,
522 1976; Vitousek et al., 2010; Butler et al., 2018; Elser et al., 2007). Recent work has also
523 explored how increasing demand for P may attenuate predicted increase in NPP
524 conceptually by comparing potential demand with potential nutrient available in the 21st
525 Century (Wieder et al., 2015b; Sun et al., 2017). Increasing numbers of land models have
526 incorporated P cycle dynamics and P limitations (Sun et al., 2021; Nakhavali et al., 2021).
527 Although both N and P limitation acts through reducing NPP, it is critical to include P cycling
528 explicitly in models since P cycle dynamics are very different from the N cycling dynamics.
529 The primary input for P is through rock weathering, which make it a very much non-
530 renewable nutrient for the terrestrial ecosystems, whereas N fixation, the primary input for
531 N, is more biologically driven. P cycling involves the transformation of various forms of P
532 through a series of biological, enzymatical and geochemical processes with the turnover

533 time ranging from seconds to millions of years. N cycle dynamics are relatively simpler, with
534 two inorganic forms and mostly biological and enzymatical processes involved. In addition,
535 the interactions between N and P cycling also points to the need to include P cycle explicitly
536 in land models. Increasing numbers of studies have shown that biological N fixation could
537 be constrained by soil P availability (Hungate et al., 2004; Reed et al., 2013; Barron et al.,
538 2008; Edwards et al., 2006; Crews et al., 2000). On the other hand, studies have also shown
539 that increases in N availability can promote phosphatase activity and enhance biochemical
540 mineralization and therefore accelerate P cycling (Mcgill and Cole, 1981; Wang et al., 2007;
541 Houlton et al., 2008; Olander and Vitousek, 2000; Treseder and Vitousek, 2001; Marklein
542 and Houlton, 2012). We will continue refine and improve the representation of the C-N-P
543 interactions in the future development of ELM.

544 Also, ILAMB, despite being a comprehensive benchmarking tool for land surface models,
545 is limited in scope in terms of the benchmarking data included. For example, Quesada et al.
546 (2012) found that the decreasing west-east gradient in productivity is mostly related to total
547 soil P across the Amazon basin. Yang et al. (2019) show that consideration of soil P
548 availability improved model simulated productivity, enabling the model to capture the
549 productivity gradient from west to east across the Amazon basin. The problem is that this
550 productivity gradient across the Amazon basin is not captured in ILAMB benchmark data so
551 the “failure” of a CN model would not be captured by ILAMB.

552 We show that the model performance generally improved with realistic P availability
553 through the implementation of a prognostic P cycle in ELM. Compared to ELMv1-CN,
554 ELMv1-CNP simulated biomass has lower bias across the tropical regions as P limitation
555 leads to lower productivity and hence lower biomass. ELMv1-CNP produces better ILAMB
556 scores on the functional relationships between GPP, LAI and other forcing variables, mainly
557 due to improved estimate of GPP and LAI in tropical regions. ELMv1-CNP also produces
558 higher ILAMB scores for the integrated benchmarks such as global net ecosystem carbon
559 balance and carbon dioxide concentration. We note that satisfactory performance for these
560 two integrated metrics is most critical to a land model in ESMs as they are most relevant to
561 the coupling between land ecosystems and radiatively-forced climate change.

562 ELMv1-CNP is not always better than ELMv1-CN from the benchmarks in the current
563 ILAMB system. One of the benefits of a multi-metric analysis package like ILAMB is that we
564 can compare performance at different levels of granularity, and it is rare that any one
565 model has uniformly improved performance over any other single model on every fine-
566 grained metric. By having multiple data sources for a given metric we can often see
567 improvement against one data source and degradation compared to another for the same
568 model output. For example, the ELMv1-CN model performs better than ELMv1-CNP for
569 ecosystem respiration when comparing the Fluxnet metric, but ELMv1-CNP does better
570 than ELMv1-CN for the GBAF metric on the same output variable. In the case of GPP and
571 NEE, although ELMv1-CN is performing better or the same as ELMv1-CNP for both Fluxnet
572 and GBAF metrics, the overall better scores of the ELMv1-CNP model for the relationship
573 metrics connected to GPP give us more confidence that ELMv1-CNP is actually an
574 improvement. Each metric has its own advantages and disadvantages, and there is still
575 considerable subjectivity in how to interpret the multi-metric collection. For example, the
576 site-level evaluations in iLAMB do not take into account site-specific disturbance histories,
577 which can be an important driver of NEE variability over time at a given site.

578
579 Although the ILAMB benchmarking system is very useful for evaluating model
580 performance from different aspects simultaneously, interpretation of ILAMB scores
581 deserves extra caution with known observational bias considered. For example, ILAMB uses
582 LAI estimated from remote sensing observations from the Moderate Resolution Imaging
583 Spectroradiometer (MODIS) as benchmarking data, while studies have suggested that
584 MODIS LAI may be biased low due to reflectance saturation in dense canopies in the
585 tropical forests (Shabanov et al., 2005; Huete et al., 2002; Kobayashi and Dye, 2005).
586 Another example is the observational data for biomass. There are significant differences
587 between the “tropical” and “GlobalCarbon” datasets and the “GeoCarbon” dataset for
588 tropical biomass, but they were given about the same default weight in the ILAMB scoring
589 system. Mitchard et al. (2014) investigated the marked differences between different
590 estimates of Amazon biomass and suggested the regional biases in some remote sensing

591 products might be due to the lack of consideration of ecological variation in tree wood
592 density and allometry. Further investigation of these datasets is needed to ensure the
593 quality of biomass benchmarking data.

594
595 The current version of ILAMB includes analysis of 28 variables using more than 60
596 datasets or data products. None of these variables, however, are directly related to nutrient
597 cycles. As more land surface models are implementing N and P dynamics, it is becoming
598 increasingly important to include metrics for nutrient stocks and fluxes. Davies-Barnard et
599 al. (2020) assessed five nitrogen-enabled land surface models in CMIP6 and called out the
600 need to have better constraints of nitrogen cycle processes. The need is equally urgent, if
601 not more, to synthesize more observations to better constrain the P cycle processes, as less
602 synthesized data are available for P. Encouragingly, recent studies have started to develop
603 observational datasets based estimate of N and P cycling on the global scale for model
604 evaluation, such as the GOLUM-CNP dataset we used in this study. We hope to highlight the
605 need and engage the broader community in developing additional nutrient datasets that
606 can be included in ILAMB.

607 Other metrics that would be useful are the responses from N and P addition
608 experiments. As Yang et al. (2014) showed, fertilization experiments at sites along the
609 Hawaii chronosequence provided a useful evaluation testbed to assess model simulated
610 responses to N and P fertilization effects. FACE experiments are useful for model evaluation
611 as shown here (section 4.2) and in other studies (Wieder et al., 2019; Davies-Barnard et al.,
612 2020). Warming studies that include an explicit focus on nutrient cycle responses will be
613 another good evaluation opportunity (Melillo et al., 2002). An existing challenge is to
614 provide a common protocol to use these types of experiments in the ILAMB benchmarking
615 system.

616

617 4.2 Evaluations using GOLUM-CNP

618

619 On the biome level ELMv1-CNP simulated nutrient use efficiencies are consistent with
620 the observation-based estimates from GOLUM-CNP. This indicates that the representation

621 of N and P cycling and C-N-P coupling is reasonable in ELMv1-CNP. In terms of nutrient
622 uptake, both show the highest N and P uptake in tropical forests, due to the high N and P
623 demand associated with high productivity. ELMv1-CNP predicted lower N uptake in the
624 tropical forests, compared to GOLUM-CNP. Nutrient uptake in ELMv1-CNP is a function of
625 nutrient availability and nutrient demand, with demand being determined by available
626 carbon for allocation, allocation fractions to different plant tissues and plant tissue
627 stoichiometry. The simulated NPP at the biome level matches well with NPP from GOLUM-
628 CNP except for Tundra (Fig. S3). The different C:N and C:P stoichiometric ratios for
629 vegetation tissues used in ELMv1-CNP and GOLUM-CNP could also contribute to the
630 difference in . C:N ratios of leaf, wood, and fine root in GOLUM-CNP are all lower than
631 ELMv1-CNP (21, 126, and 40 in GOLUM vs 30, 500, and 42 in ELMv1-CNP). This suggests for
632 given amount of carbon allocation, N uptake would be lower in ELMv1-CNP. Soil P
633 availability might be overestimated considering ELMv1-CNP estimated P leaching is much
634 lower than the estimate of Wang et al. (2018), therefore leading to relatively higher P
635 uptake in ELMv1-CNP. Differences in allocation factors could also be contributing to the
636 differences in nutrient uptake between ELMv1-CNP and GOLUM-CNP. For example, the
637 mean allocation fraction to fine root is higher in GOLUM-CNP compared to ELM-CNP, while
638 allocation fraction to leaf is lower in GOLUM-CNP, particularly in forest ecosystems (Fig. S4
639 and S6). GOLUM-CNP also has higher NPP allocation fraction to woody biomass in boreal
640 forests (Fig. S5)

641

642 **4.3. Evaluations using CO₂ manipulation experiments**

643 Our simulated large increase in GPP with CO₂ enrichment (23%) is in agreement with
644 field observations that photosynthetic assimilation increased 28% under elevated CO₂
645 (Ainsworth and Long, 2005). Our simulated 26% increase in NPP is higher than the 17%
646 increase in observed increase in dry matter production in the FACE experiments (Ainsworth
647 and Long, 2005; Wieder et al., 2019). Our simulated 18% increase in biomass is higher than
648 the estimates from Terrer et al. (2019), which provides a data-driven estimate of global CO₂
649 fertilization effect on biomass and show a relative increase in biomass of 12±3% for a 250

650 ppm CO₂ increase. A meta-analysis of woody plants responses to elevated CO₂ shows a
651 mean effects of 22.3% on biomass (Baig et al., 2015). Among CLM4, CLM4.5 and CLM5,
652 ELMv1-CNP is more comparable to CLM5 with a strong simulated response of GPP, NPP, and
653 vegetation carbon in response to CO₂ enrichment, while CLM4 and CLM4.5 showed very
654 weak CO₂ effects (Wieder et al., 2019).

655 The much stronger sensitivity of photosynthesis to elevated CO₂ in ELMv1-CNP is due to
656 the removal of instantaneous downregulation of photosynthesis as a response to nutrient
657 limitation. The instantaneous downregulation assumption in CLM4 and CLM4.5 has been
658 shown to be inconsistent with experimental results (Metcalf et al., 2017). Despite large
659 uncertainty, it is encouraging that simulated NSC response to elevated CO₂ is largely
660 consistent with the observational data (Fig. 7). The low sensitivity of LAI in ELMv1-CNP is
661 also consistent with field observations. Our results suggest the assumption we made
662 regarding the fate of photosynthate is reasonable. Yang et al. (2016) showed that enhanced
663 phosphatase enzyme production response to increasing CO₂ could have important impacts
664 on P availability and sustain forest productivity under elevated CO₂. In simulating the
665 planned free-air CO₂ enrichment experiment AmazonFACE, ELMv1-CNP simulated
666 phosphatase activity increased about 20% over 15 years (Fleischer et al., 2019). Here we
667 show that introduction of NSC pools further improve the response of vegetation processes
668 to changes in P availability and P limitation.

669
670 Our findings are consistent with field studies that show the strong increase of NSC under
671 elevated CO₂ condition (eCO₂), particularly when nutrient availability is low (Wong, 1990;
672 Körner et al. (2005). Several studies evaluating CLM4.5 using carbon isotope data also
673 suggested that model performance would be better with the introduction of an NSC pool
674 (Mao et al., 2016; Raczka et al., 2016; Duarte et al., 2017). However, large uncertainties
675 remain regarding the turnover rate of the NSC pool. Further synthesis of field
676 measurements on NSC in CO₂ enrichment experiments are needed to evaluate and
677 constrain the representation of NSC in models.

678 Our simulated strong sensitivity of photosynthesis to CO₂ enrichment is consistent with
679 recent studies that show large GPP growth during the twentieth century (Campbell et al.,
680 2017; Haverd et al., 2020; Ehlers et al., 2015). Ellsworth et al (2017) also showed a large
681 increase of photosynthesis in response to elevated CO₂ in a temperate forest FACE
682 experiment.

683 The increased sensitivity of GPP and NPP to CO₂ enrichment in ELMv1-CNP, compared
684 with the predecessors CLM 4 and CLM4.5, will very likely reduce the bias in the atmospheric
685 fraction of human CO₂ emissions in previous coupled simulations as noted by Hoffman et al.
686 (2014). In fact, CO₂ concentration metrics in ILAMB, which translate model simulated NEE
687 into atmospheric CO₂ signal using an atmospheric transport model (Collier et al., 2018), is
688 intended for the evaluation of this sensitivity. The inferred atmospheric CO₂ concentration
689 from ELM v1 is very reasonable compared with observed NOAA flask data (Fig. S7 and S8).

690

691 **4.4. Model estimated carbon, nitrogen, and phosphorus pools and fluxes**

692 Global C, N, and P pools in our ELMv1-CNP simulation are in good agreement with
693 recent independent global estimates, indicating that ELMv1-CNP is capable of simulating
694 the contemporary C, N and P cycles. In Yang et al. (2019) it was shown that introduction of
695 more realistic mortality processes improved the model representation of longitudinal
696 spatial patterns of biomass across the Amazon basin. Here we show that an overall high
697 bias in biomass production is corrected through limits of vegetation production in response
698 to P availability, without compromising the improved spatial gradients obtained through
699 the mortality mechanism. It is worth mentioning that our understanding of nutrient stocks
700 and fluxes is much less advanced in comparison with the global C cycle. This has been
701 increasingly acknowledged for the global N cycle as increasing numbers of land surface
702 models have incorporated N cycle dynamics and C-N interactions (Zaehle et al., 2010;
703 Wieder et al., 2019; Davies-Barnard et al., 2020; Smith et al., 2014; Sellar et al., 2019; Goll
704 et al., 2017a; Gerber et al., 2010). Biological N fixation and N-use efficiency have been
705 identified as the key processes that need to be better constrained for land surface models
706 (Davies-Barnard et al., 2020).

707 Our understanding of P stocks and fluxes are even less advanced than that for the N
708 cycle, as shown in this study and other modeling studies that include P as a limiting
709 nutrient. This is mainly due to: (1) various forms of P with different level of availability for
710 plants and microbes, (2) geochemical processes in conjunction with biological processes
711 controlling P availability, and (3) technical challenges in measuring soil P. For example,
712 Hedley fractionation data provide a comprehensive picture of different P forms in soils and
713 has been used for model evaluation and/or initialization in all the land surface models that
714 include a prognostic phosphorus cycle (Wang et al., 2010; Goll et al., 2012; Yang et al.,
715 2014; Yang et al., 2019). However, this extraction method is time-consuming and
716 challenging, and not many routine measurements have been made using this technique.
717 As such, observational estimates of P pools and fluxes are extremely limited. Although
718 recent global Hedley database development (Yang and Post, 2011; Hou et al., 2018) has
719 been helpful in global model development and evaluation, more observational data on P
720 stocks and fluxes are needed to better constrain P-enabled models.

721

722

723 **4.5. Effects of accounting for the P cycle dynamics on simulated carbon balance**

724 **4.5.1. Spatial variation of nutrient limitation**

725 Our simulated nutrient limitation pattern broadly agrees with the findings from Elser et
726 al. (2007) which supports the generally accepted notion that tropical ecosystems residing
727 on highly weathered soils are P limited (Walker and Syers, 1976; Lebauer and Treseder,
728 2008). A recent study that predicted spatial patterns of N and P limitation using the ratios
729 of leaf N and P resorption efficiencies also found a shift from P limitation to N limitation
730 with increasing latitude (Du et al., 2020). Lebauer and Treseder (2008) showed that N
731 limitation is widespread, even in tropical regions. This is consistent with our model
732 simulations which show that although P is more limiting in tropical forests, N is also a
733 limiting nutrient. The geographic distribution of nutrient limitation is generally in
734 agreement with that from Goll et al. (2012) and Wang et al. (2010). Goll et al. (2012)
735 suggests that P limits C uptake mainly in low latitude regions and high latitudes, while N is

736 the limiting nutrient in temperate regions. It is worth mentioning that in Goll et al. (2012) N
737 and P limitation generally have distinct geographic occurrence while this study suggests NP
738 co-limitation occurs in many parts of the world. Wang et al. (2010) also showed that
739 productivity in tropical forests and savanna is limiting by P, while most other biomes are
740 limited by N. This is broadly consistent with our results but with a few key differences.
741 Wang et al. (2010) suggests that P is the limiting nutrient for savannas, whereas our results
742 show savannas are more limited by N. This may have to do with the lack of representation
743 of fire disturbance in Wang et al. (2010). Savannas are subject to regular wildfires, which
744 could have significant effects on nutrient cycle dynamics and nutrient limitation. For
745 example, it has been suggested that while combustion causes significant gaseous losses of
746 N from burned ecosystems, P is largely retained as ash (Herbert et al., 2003). Braakhekke et
747 al (2017) also showed that there are strong losses of N due to fire. Furthermore, Wang et
748 al. (2010) suggested that tropical forests are limited only by P, not by N, whereas our
749 results indicate that N and P both limit tropical forest productivity, although P limitation is
750 more dominant in most of the lowland tropical forests. This is consistent with a recent
751 meta-analysis of nutrient fertilization experiments in tropical forests (Wright et al., 2018).

752

753 **4.5.2. The implications for global carbon cycle and climate**

754 Historical C accumulation is a result of many complex and sometimes counteracting
755 processes controlling C fluxes and stocks (Lawrence et al., 2019), including accumulation of
756 carbon on land due to CO₂ fertilization, accumulation due to nitrogen deposition, carbon
757 fluxes due to climate variability and climate change, and losses and gains due to land cover
758 conversion and regrowth following historical land cover changes (LULCC fluxes). Over the
759 long term, two of the dominant processes controlling C accumulation in terrestrial
760 ecosystems are C emissions due to LULCC and C uptake due to the CO₂ fertilization effect. P
761 cycle dynamics have important impacts on both of these processes, but with opposite sign.
762 Globally, considering P cycle dynamics leads to lower carbon emissions associated with
763 deforestation by about 11% (161.21 Pg in CN vs 143.89 in CNP). Conversely, CO₂
764 fertilization at the global scale is reduced by 20% when P limitation is included during the

765 historical time period (134 Pg C vs 108 Pg C). In general, the ELMv1-CN simulation shows a
766 CO₂ fertilization effect on biomass that is too strong, which leads to a stronger than
767 observed carbon sink compared to observational constraints from both Hoffman et al.
768 (2014) and Le Quere et al. (2016). ELMv1-CN simulation also produces stronger carbon
769 emissions from LULCC due to having higher biomass compared to ELMv1-CNP. The CO₂
770 fertilization effect in the ELMv1-CN simulations is strong enough to overcome the LULCC
771 losses with the net result being too large of a sink throughout the historical time period for
772 the CN model. Both model configurations lose carbon too slowly due to LULCC in the period
773 from 1850–1940, when compared to the Hoffman et al. (2014) global estimate. Both
774 models also predict continued losses over the period 1940–1965, while the Hoffman et al.
775 (2014) estimate switches from net carbon loss to net carbon accumulation around 1940.
776 These are clearly shown in Fig. S9, which shows the time series of simulated change in land
777 carbon storage in response to changes in CO₂, LULCC, N deposition, and climate during
778 1850-2010. The ELMv1-CN and ELMv1-CNP models are similar to many other CMIP6
779 models with respect to this bias in the timing of transition from net land carbon source to
780 net land sink as shown in our ILAMB analysis of other land models in CMIP6.

781
782 We also note that, over the historical time period, P became more limiting as simulated
783 historical C accumulations became increasingly divergent between CN and CNP simulations.
784 This is mainly caused by stimulated plant productivity under higher atmospheric CO₂, which
785 leads to higher plant demand for P that is not balanced by increased supply of newly
786 mineralized P from the soil. This is consistent with other global modeling studies with
787 explicit representation of P cycle dynamics (Goll et al., 2012; Zhang et al., 2014), as well as
788 diagnostic studies that evaluated how CO₂ fertilization simulated by CMIP5 models could
789 be constrained by soil P availability using a mass balance approach (Wieder et al., 2015b;
790 Sun et al., 2017). Taken together, the limiting effect of P availability on C uptake will likely
791 have substantial consequences for projections of future C uptake.

792
793

794 **4.6. Limitations and future development**

795 While the ELMv1-CNP simulations presented here show that the model is capable of
796 representing contemporary C, N and P stocks and fluxes and capturing the observed
797 ecosystem responses to changes in atmospheric CO₂, the current configuration does have
798 limitations.

799 While the model represents disturbances such as fire and the interactions between
800 disturbances and nutrient cycle dynamics, these interactions and how they affect carbon
801 cycle processes have not been well constrained with observational data. There is a growing
802 body of literature investigating the biogeochemical signature of fire. For example, a meta-
803 analysis by Butler et al. (2018) shows that fire led to significantly higher concentration of
804 soil mineral P and lower soil and litter C:P and N:P ratios, therefore decoupling the P cycle
805 from the C and N cycles. We will take advantage of these recent findings to improve model
806 fidelity on this front.

807 Another area that needs to be improved is the treatment of N fixation and how that is
808 linked to P availability. N fixation in ELMv1-CNP is represented as a function of NPP
809 (Cleveland et al., 1999). While providing a reasonable global estimate of N fixation, the
810 approach ignores existing mechanistic understanding of nitrogen fixation processes
811 (Wieder et al., 2015a). Furthermore, several lines of evidence suggest that both symbiotic
812 and free-living N fixation rates depend on the availability of other elements, such as P and
813 molybdenum (Reed et al., 2013; Nasto et al., 2014). N fixation could have important
814 implications for the spatial distribution of N limitation vs P limitation. In the future we plan
815 to have a more mechanistic representation of N fixation in ELM.

816 In ELMv1-CNP, P limitation is represented by downregulating plant growth when P
817 demand is greater than soil P availability. The mechanisms by which P fundamentally limits
818 ecosystem productivity remain uncertain (Jiang et al., 2019). Some studies proposed that
819 there are linear or log-linear relationships between leaf P concentration and
820 photosynthetic parameters, although the relationship has been shown to be weak (Walker
821 et al., 2014). P fertilization experiments in P limited ecosystems do not support this
822 proposed relationship. A P fertilization experiment on highly weathered soils in Australia

823 showed that although leaf P concentration increased significantly (+50%) compared to
824 unfertilized trees, photosynthetic capacity was unaffected (Crous et al., 2015).
825 Another fertilization experiment in Hawaii showed that the increase of aboveground NPP
826 with P fertilization was caused mainly by increases in LAI instead of photosynthesis per unit
827 leaf area (Herbert and Fownes, 1995). Further laboratory and field experiments are needed
828 to help us better understand and represent the role of P in photosynthesis. Investigating
829 the detailed mechanisms through which leaf P concentration affects photosynthesis is an
830 active field of research (Jiang et al., 2019; Norby et al., 2017; Crous et al., 2015), and
831 representing these relationships in land models remains an outstanding challenge.

832 Uncertainty also remains regarding the ELMv1-CNP representation of sorption dynamics
833 and biochemical mineralization and their responses to changes in atmospheric CO₂ and
834 climate (Fleischer et al., 2019). Motivated by our previous modeling studies, several recent
835 field studies have started focusing on improving our mechanistic understanding and
836 providing quantitative relationships for modelling these processes (Cabugao et al., 2017;
837 Brenner et al., 2019). A recent study that upscaled site-measurements of potential
838 phosphatase activity to continental Europe using machine learning technique provides a
839 potential pathway toward generating benchmark data for biochemical mineralization on
840 regional to global scale (Sun et al., 2020). ELMv1-CNP is likely underestimating P leaching,
841 in comparison to the estimate of Wang et al. (2018), which could contribute to the
842 underestimate of P uptake and overestimate of land carbon sink. We will further improve
843 the representation of P leaching in ELMv1. There are other mechanisms that could sustain
844 productivity with increasing P limitation but were not considered in ELMv1-CNP, such as
845 flexible stoichiometry and dynamic allocation. These will be investigated further in future
846 versions of E3SM. However, as Fleischer et al. (2019) pointed out, since plant N:P ratios in
847 highly P limited tropical forests are already at the high end of the observed spectrum, the
848 role of stoichiometry plasticity in sustaining tropical productivity could be limited.

849 While the representation of NSC has helped ELMv1-CNP to capture the interannual
850 variability of atmospheric CO₂ and to generate ecosystem responses to elevated CO₂
851 consistent with FACE measurements, the sizes and turnover times of NSC pools are not well

852 constrained. We will synthesize limited measurements on NSC from literature that include
853 observational and experimental data as well as measurements from isotopic studies to
854 better understand the dynamics of the NSC pool and to evaluate and refine its
855 representation in ELM. We also advocate for more measurements on NSC and how they
856 respond to environmental changes in diverse ecosystems to have a more complete
857 understanding and quantification of NSC.

858 Finally, although models such as ELMv1-CNP and CLM5 perform similarly when
859 evaluated against present-day metrics as gathered in ILAMB, we expect that the
860 differences among models in their representation of observed processes and in their
861 assumptions about how changes in atmospheric composition and climate will impact
862 ecosystem processes will lead to diverging predictions under future climate scenarios. We
863 will explore those differences and their consequences in future work.

864

865 **5. Conclusions**

866 In this study, we provide an evaluation of ELMv1-CNP using the ILAMB benchmarking
867 system, comparison with CO₂ manipulation experiments, and comparison with other
868 observational and modeling studies. Benchmarking with ILAMB indicates ELMv1-CNP
869 produces realistic estimates of present-day carbon pools and fluxes. Compared to a
870 simulation with optimal P availability, ELMv1-CNP produces better performance,
871 particularly for the metrics that are most relevant to land-atmosphere exchange. Our
872 results from CO₂ manipulation experiments suggest that ELMv1-CNP is able to capture
873 observed responses to elevated CO₂, including those for GPP, NPP, vegetation C, and LAI.
874 Further analysis suggests that the introduction of a non-structural carbon pool in ELMv1-
875 CNP is largely responsible for these improvements. Evaluating global C, N, and P pools and
876 fluxes in the context of literature values suggests that ELMv1-CNP provides a reasonable
877 representation of contemporary global scale C, N and P cycles.

878 We highlight the data needs for global land model evaluation, particularly the need for
879 more synthesis datasets on nutrient pools and fluxes, as well as observations from
880 manipulation experiments that provide additional benchmark data for nutrient cycle

881 evaluation. This need is becoming increasingly pressing as more land models are including N
882 and P cycle dynamics and C-N-P interactions. We also identify challenges in constraining P
883 cycle dynamics and point to the need for soil P measurements.

884 Our simulations suggest, probably not surprisingly, that in general P is the more limiting
885 nutrient in the tropical regions while N is more limiting in the middle to high latitudes.
886 However, our results also suggest widespread N and P colimitation, even in the tropical
887 regions where P limitation is more dominant. Our results show that C sources and sinks are
888 significantly affected by P limitation, as the historical CO₂ fertilization effect was reduced by
889 20% and C emission due to LULCC was 11% lower when P limitation was considered. We
890 conclude that introduction of P cycle dynamics and C-N-P coupling will likely have
891 substantial consequences for projections of future C uptake.

892

893 Acknowledgement:

894 This research was supported as part of the Energy Exascale Earth System Model (E3SM) project,
895 funded by the U.S. Department of Energy, Office of Science, Office of Biological and
896 Environmental Research. This research was also supported by the Oak Ridge National
897 Laboratory's (ORNL) Terrestrial Ecosystem Science Focus Area (TES SFA). F. M. Hoffman was
898 supported by the Reducing Uncertainties in Biogeochemical Interactions through Synthesis and
899 Computation Scientific Focus Area (RUBISCO SFA), which is sponsored by the Regional and
900 Global Model Analysis (RGMA) Program in the Climate and Environmental Sciences Division
901 (CESD) of the Office of Biological and Environmental Research (BER) in the U.S. Department of
902 Energy Office of Science. We thank Min Xu for his help in running ILAMB. The E3SM model can
903 be accessed at <https://www.osti.gov/doecode/biblio/10475> (doi:
904 [10.11578/E3SM/dc.20180418.36](https://doi.org/10.11578/E3SM/dc.20180418.36)). The input data is available at
905 <https://web.lcrc.anl.gov/public/e3sm/inputdata/>.

906 The model outputs used in this study can be downloaded at the website:
907 <https://doi.org/10.6084/m9.figshare.12021348>.

908

909

910 References:

911 Ainsworth, E. A. and Long, S. P.: What have we learned from 15 years of free-air CO₂
912 enrichment (FACE)? A meta-analytic review of the responses of photosynthesis, canopy
913 properties and plant production to rising CO₂, *New phytologist*, 165, 351-372, 2005.
914 Aragão, L., Malhi, Y., Metcalfe, D., Silva-Espejo, J., Jimenez, E., Navarrete, D., Almeida, S.,
915 Costa, A., Salinas, N., and Phillips, O.: Above-and below-ground net primary productivity across
916 ten Amazonian forests on contrasting soils, *Biogeosciences*, 6, 2759-2778, 2009.

917 Arora, V. K., Boer, G. J., Friedlingstein, P., Eby, M., Jones, C. D., Christian, J. R., Bonan, G.,
918 Bopp, L., Brovkin, V., and Cadule, P.: Carbon-concentration and carbon-climate feedbacks in
919 CMIP5 Earth system models, *Journal of Climate*, 26, 5289-5314, 2013.

920 Arora, V. K., Katavouta, A., Williams, R. G., Jones, C. D., Brovkin, V., Friedlingstein, P.,
921 Schwinger, J., Bopp, L., Boucher, O., and Cadule, P.: Carbon-concentration and carbon-climate
922 feedbacks in CMIP6 models and their comparison to CMIP5 models, *Biogeosciences*, 17, 4173-
923 4222, 2020.

924 Avitabile, V., Herold, M., Heuvelink, G. B., Lewis, S. L., Phillips, O. L., Asner, G. P., Armston,
925 J., Ashton, P. S., Banin, L., and Bayol, N.: An integrated pan-tropical biomass map using
926 multiple reference datasets, *Global change biology*, 22, 1406-1420, 2016.

927 Baig, S., Medlyn, B. E., Mercado, L. M., and Zaehle, S.: Does the growth response of woody
928 plants to elevated CO₂ increase with temperature? A model-oriented meta-analysis, *Global
929 change biology*, 21, 4303-4319, 2015.

930 Barron, A. R., Wurzburger, N., Bellenger, J. P., Wright, S. J., Kraepiel, A. M., and Hedin, L. O.:
931 Molybdenum limitation of asymbiotic nitrogen fixation in tropical forest soils, *Nature
932 Geoscience*, 2, 42-45, 2008.

933 Batjes, N. H.: Total carbon and nitrogen in the soils of the world, *European journal of soil
934 science*, 65, 10-21, 2014.

935 Beer, C., Reichstein, M., Tomelleri, E., Ciais, P., Jung, M., Carvalhais, N., Rödenbeck, C.,
936 Arain, M. A., Baldocchi, D., and Bonan, G. B.: Terrestrial gross carbon dioxide uptake: global
937 distribution and covariation with climate, *Science*, 329, 834-838, 2010.

938 Bonan, G. B., Lombardozzi, D. L., Wieder, W. R., Oleson, K. W., Lawrence, D. M., Hoffman, F.
939 M., and Collier, N.: Model structure and climate data uncertainty in historical simulations of the
940 terrestrial carbon cycle (1850–2014), *Global Biogeochemical Cycles*, 33, 1310-1326, 2019.

941 Bonan, G. B., Lawrence, P. J., Oleson, K. W., Levis, S., Jung, M., Reichstein, M., Lawrence, D.
942 M., and Swenson, S. C.: Improving canopy processes in the Community Land Model version 4
943 (CLM4) using global flux fields empirically inferred from FLUXNET data, *Journal of
944 Geophysical Research: Biogeosciences*, 116, 2011.

945 Brenner, J., Porter, W., Phillips, J. R., Childs, J., Yang, X., and Mayes, M. A.: Phosphorus
946 sorption on tropical soils with relevance to Earth system model needs, *Soil research*, 57, 17-27,
947 2019.

948 Burrows, S., Maltrud, M., Yang, X., Zhu, Q., Jeffery, N., Shi, X., Ricciuto, D., Wang, S., Bisht,
949 G., and Tang, J.: The DOE E3SM v1.1 Biogeochemistry Configuration: Description and
950 Simulated Ecosystem-Climate Responses to Historical Changes in Forcing, *Journal of Advances
951 in Modeling Earth Systems*, 12, e2019MS001766, 2020.

952 Butler, O. M., Elser, J. J., Lewis, T., Mackey, B., and Chen, C.: The phosphorus-rich signature of
953 fire in the soil-plant system: a global meta-analysis, *Ecology letters*, 21, 335-344, 2018.

954 Cabugao, K. G., Timm, C. M., Carrell, A. A., Childs, J., Lu, T.-Y. S., Pelletier, D. A., Weston,
955 D. J., and Norby, R. J.: Root and rhizosphere bacterial phosphatase activity varies with tree
956 species and soil phosphorus availability in Puerto Rico tropical forest, *Frontiers in plant science*,
957 8, 1834, 2017.

958 Campbell, J., Berry, J., Seibt, U., Smith, S. J., Montzka, S., Launois, T., Belviso, S., Bopp, L.,
959 and Laine, M.: Large historical growth in global terrestrial gross primary production, *Nature*,
960 544, 84-87, 2017.

961 Cleveland, C., Townsend, A., Schimel, D., Fisher, H., Howarth, R., Hedin, L., Perakis, S., Latty,
 962 E., Von Fischer, J., and Elseroad, A.: Global patterns of terrestrial biological nitrogen (N₂)
 963 fixation in natural ecosystems, *Global Biogeochemical Cycles*, 13, 623-645, 1999.
 964 Collier, N., Hoffman, F. M., Lawrence, D. M., Keppel-Aleks, G., Koven, C. D., Riley, W. J.,
 965 Mu, M., and Randerson, J. T.: The International Land Model Benchmarking (ILAMB) system:
 966 design, theory, and implementation, *Journal of Advances in Modeling Earth Systems*, 10, 2731-
 967 2754, 2018.
 968 Crews, T. E., Farrington, H., and Vitousek, P. M.: Changes in asymbiotic, heterotrophic nitrogen
 969 fixation on leaf litter of *Metrosideros polymorpha* with long-term ecosystem development in
 970 Hawaii, *Ecosystems*, 3, 386-395, 2000.
 971 Crous, K. Y., Osvaldsson, A., and Ellsworth, D. S.: Is phosphorus limiting in a mature
 972 *Eucalyptus* woodland? Phosphorus fertilisation stimulates stem growth, *Plant and soil*, 391, 293-
 973 305, 2015.
 974 Davies-Barnard, T. and Friedlingstein, P.: The Global Distribution of Biological Nitrogen
 975 Fixation in Terrestrial Natural Ecosystems, *Global Biogeochemical Cycles*, 34,
 976 e2019GB006387, 10.1029/2019gb006387, 2020.
 977 Davies-Barnard, T., Meyerholt, J., Zaehle, S., Friedlingstein, P., Brovkin, V., Fan, Y., Fisher, R.
 978 A., Jones, C. D., Lee, H., and Peano, D.: Nitrogen cycling in CMIP6 land surface models:
 979 Progress and limitations, *Biogeosciences Discussions*, 2020.
 980 DeFries, R., Field, C., Fung, I., Collatz, G., and Bounoua, L.: Combining satellite data and
 981 biogeochemical models to estimate global effects of human-induced land cover change on
 982 carbon emissions and primary productivity, *Global biogeochemical cycles*, 13, 803-815, 1999.
 983 Du, E., Terrer, C., Pellegrini, A. F., Ahlström, A., van Lissa, C. J., Zhao, X., Xia, N., Wu, X.,
 984 and Jackson, R. B.: Global patterns of terrestrial nitrogen and phosphorus limitation, *Nature*
 985 *Geoscience*, 13, 221-226, 2020.
 986 Duarte, H. F., Raczka, B. M., Ricciuto, D. M., Lin, J. C., Koven, C. D., Thornton, P. E.,
 987 Bowling, D. R., Lai, C.-T., Bible, K. J., and Ehleringer, J. R.: Evaluating the Community Land
 988 Model (CLM4. 5) at a coniferous forest site in northwestern United States using flux and carbon-
 989 isotope measurements, *Biogeosciences (Online)*, 14, 2017.
 990 Edwards, E., McCaffery, S., and Evans, J.: Phosphorus availability and elevated CO₂ affect
 991 biological nitrogen fixation and nutrient fluxes in a clover dominated sward, *New Phytologist*,
 992 169, 157-167, 2006.
 993 Ehlers, I., Augusti, A., Betson, T. R., Nilsson, M. B., Marshall, J. D., and Schleucher, J.:
 994 Detecting long-term metabolic shifts using isotopomers: CO₂-driven suppression of
 995 photorespiration in C₃ plants over the 20th century, *Proceedings of the National Academy of*
 996 *Sciences*, 112, 15585-15590, 2015.
 997 Ellsworth, D. S., Anderson, I. C., Crous, K. Y., Cooke, J., Drake, J. E., Gherlenda, A. N.,
 998 Gimeno, T. E., Macdonald, C. A., Medlyn, B. E., and Powell, J. R.: Elevated CO₂ does not
 999 increase eucalypt forest productivity on a low-phosphorus soil, *Nature Climate Change*, 7, 279-
 1000 282, 2017.
 1001 Elser, J. J., Bracken, M. E. S., Cleland, E. E., Gruner, D. S., Harpole, W. S., Hillebrand, H.,
 1002 Ngai, J. T., Seabloom, E. W., Shurin, J. B., and Smith, J. E.: Global analysis of nitrogen and
 1003 phosphorus limitation of primary producers in freshwater, marine and terrestrial ecosystems,
 1004 *Ecology Letters*, 10, 1135-1142, 10.1111/j.1461-0248.2007.01113.x, 2007.

1005 Erb, K.-H., Kastner, T., Plutzer, C., Bais, A. L. S., Carvalhais, N., Fetzel, T., Gingrich, S.,
1006 Haberl, H., Lauk, C., and Niedertscheider, M.: Unexpectedly large impact of forest management
1007 and grazing on global vegetation biomass, *Nature*, 553, 73-76, 2018.

1008 Finzi, A. C., Norby, R. J., Calfapietra, C., Gallet-Budynek, A., Gielen, B., Holmes, W. E.,
1009 Hoosbeek, M. R., Iversen, C. M., Jackson, R. B., and Kubiske, M. E.: Increases in nitrogen
1010 uptake rather than nitrogen-use efficiency support higher rates of temperate forest productivity
1011 under elevated CO₂, *Proceedings of the National Academy of Sciences*, 104, 14014-14019,
1012 2007.

1013 Fleischer, K., Rammig, A., De Kauwe, M. G., Walker, A. P., Domingues, T. F., Fuchslueger, L.,
1014 Garcia, S., Goll, D. S., Grandis, A., and Jiang, M.: Amazon forest response to CO₂ fertilization
1015 dependent on plant phosphorus acquisition, *Nature Geoscience*, 12, 736-741, 2019.

1016 Friedlingstein, P., Jones, M., O'Sullivan, M., Andrew, R., Hauck, J., Peters, G., Peters, W.,
1017 Pongratz, J., Sitch, S., and Le Quéré, C.: Global carbon budget 2019, *Earth System Science Data*,
1018 11, 1783-1838, 2019.

1019 Gerber, S., Hedin, L. O., Oppenheimer, M., Pacala, S. W., and Shevliakova, E.: Nitrogen cycling
1020 and feedbacks in a global dynamic land model, *Global Biogeochemical Cycles*, 24, GB1001,
1021 10.1029/2008gb003336, 2010.

1022 Ghimire, B., Riley, W. J., Koven, C. D., Mu, M., and Randerson, J. T.: Representing leaf and
1023 root physiological traits in CLM improves global carbon and nitrogen cycling predictions,
1024 *Journal of Advances in Modeling Earth Systems*, 8, 598-613, 2016.

1025 Goll, D., Winkler, A., Raddatz, T., Dong, N., Prentice, I., Ciais, P., and Brovkin, V.: Carbon–
1026 nitrogen interactions in idealized simulations with JSBACH (version 3.10), *Geosci. Model Dev.*,
1027 10, 2009–2030, 2017a.

1028 Goll, D., Brovkin, V., Parida, B., Reick, C., Kattge, J., Reich, P., van Bodegom, P., and
1029 Niinemets, U.: Nutrient limitation reduces land carbon uptake in simulations with a model of
1030 combined carbon, nitrogen and phosphorus cycling, *Biogeosciences*, 9, 3547-3569, 2012.

1031 Goll, D., Vuichard, N., Maignan, F., Jornet-Puig, A., Sardans, J., Violette, A., Peng, S., Sun, Y.,
1032 Kvakic, M., and Guimberteau, M.: A representation of the phosphorus cycle for ORCHIDEE
1033 (revision 4520), 2017b.

1034 Haverd, V., Smith, B., Canadell, J. G., Cuntz, M., Mikaloff-Fletcher, S., Farquhar, G.,
1035 Woodgate, W., Briggs, P. R., and Trudinger, C. M.: Higher than expected CO₂ fertilization
1036 inferred from leaf to global observations, *Global change biology*, 26, 2390-2402, 2020.

1037 Herbert, D. A. and Fownes, J. H.: Phosphorus limitation of forest leaf area and net primary
1038 production on a highly weathered soil, *Biogeochemistry*, 29, 223-235, 1995.

1039 Herbert, D. A., Williams, M., and Rastetter, E. B.: A model analysis of N and P limitation on
1040 carbon accumulation in Amazonian secondary forest after alternate land-use abandonment,
1041 *Biogeochemistry*, 65, 121-150, 2003.

1042 Hoffman, F., Koven, C., Keppel-Aleks, G., Lawrence, D., Riley, W., Randerson, J., Ahlström,
1043 A., Abramowitz, G., Baldocchi, D., and Best, M.: International land model benchmarking
1044 (ILAMB) 2016 Workshop Report, US Department of Energy, Office of Science, 10, 1330803,
1045 2017.

1046 Hoffman, F. M., Randerson, J. T., Arora, V. K., Bao, Q., Cadule, P., Ji, D., Jones, C. D.,
1047 Kawamiya, M., Khatiwala, S., and Lindsay, K.: Causes and implications of persistent
1048 atmospheric carbon dioxide biases in Earth System Models, *Journal of Geophysical Research:*
1049 *Biogeosciences*, 119, 141-162, 2014.

1050 Hou, E., Tan, X., Heenan, M., and Wen, D.: A global dataset of plant available and unavailable
1051 phosphorus in natural soils derived by Hedley method, *Scientific data*, 5, 180166, 2018.

1052 Hou, E., Luo, Y., Kuang, Y., Chen, C., Lu, X., Jiang, L., Luo, X., and Wen, D.: Global meta-
1053 analysis shows pervasive phosphorus limitation of aboveground plant production in natural
1054 terrestrial ecosystems, *Nature Communications*, 11, 1-9, 2020.

1055 Houghton, R. A.: The contemporary carbon cycle, *Treatise on geochemistry*, 8, 473-513, 2003.

1056 Houlton, B. Z., Wang, Y.-P., Vitousek, P. M., and Field, C. B.: A unifying framework for
1057 dinitrogen fixation in the terrestrial biosphere, *Nature*, 454, 327-330, 10.1038/nature07028,
1058 2008.

1059 Huete, A., Didan, K., Miura, T., Rodriguez, E. P., Gao, X., and Ferreira, L. G.: Overview of the
1060 radiometric and biophysical performance of the MODIS vegetation indices, *Remote sensing of*
1061 *environment*, 83, 195-213, 2002.

1062 Hungate, B. A., Dukes, J. S., Shaw, M. R., Luo, Y., and Field, C. B.: Nitrogen and climate
1063 change, *Science*, 302, 1512-1513, 2003.

1064 Hungate, B. A., Stiling, P. D., Dijkstra, P., Johnson, D. W., Ketterer, M. E., Hymus, G. J.,
1065 Hinkle, C. R., and Drake, B. G.: CO₂ elicits long-term decline in nitrogen fixation, *Science*, 304,
1066 1291, 2004.

1067 Jahnke, R.: The phosphorus cycle, *Global Biogeochemical Cycles*, 301-315, 1992.

1068 Jiang, M., Caldararu, S., Zaehle, S., Ellsworth, D. S., and Medlyn, B. E.: Towards a more
1069 physiological representation of vegetation phosphorus processes in land surface models, *New*
1070 *Phytologist*, 222, 1223-1229, 2019.

1071 Jobbágy, E. G. and Jackson, R. B.: The vertical distribution of soil organic carbon and its relation
1072 to climate and vegetation, *Ecological applications*, 10, 423-436, 2000.

1073 Joiner, J., Yoshida, Y., Zhang, Y., Duveiller, G., Jung, M., Lyapustin, A., Wang, Y., and Tucker,
1074 C. J.: Estimation of terrestrial global gross primary production (GPP) with satellite data-driven
1075 models and eddy covariance flux data, *Remote Sensing*, 10, 1346, 2018.

1076 Jones, C. D., Arora, V., Friedlingstein, P., Bopp, L., Brovkin, V., Dunne, J., Graven, H.,
1077 Hoffman, F., Ilyina, T., and John, J. G.: C4MIP—The coupled climate–carbon cycle model
1078 intercomparison project: Experimental protocol for CMIP6, *Geoscientific Model Development*,
1079 9, 2853-2880, 2016.

1080 Jung, C.-G., Shin, H.-J., Park, M.-J., Joh, H.-K., and Kim, S.-J.: Evaluation of MODIS Gross
1081 Primary Production (GPP) by Comparing with GPP from CO₂ Flux Data Measured in a Mixed
1082 Forest Area, *Journal of the Korean Society of Agricultural Engineers*, 53, 1-8, 2011.

1083 Kobayashi, H. and Dye, D. G.: Atmospheric conditions for monitoring the long-term vegetation
1084 dynamics in the Amazon using normalized difference vegetation index, *Remote Sensing of*
1085 *Environment*, 97, 519-525, 2005.

1086 Köchy, M., Hiederer, R., and Freibauer, A.: Global distribution of soil organic carbon—Part 1:
1087 Masses and frequency distributions of SOC stocks for the tropics, permafrost regions, wetlands,
1088 and the world, *Soil*, 1, 351-365, 2015.

1089 Koven, C., Riley, W., Subin, Z., Tang, J., Torn, M., Collins, W., Bonan, G., Lawrence, D., and
1090 Swenson, S.: The effect of vertically resolved soil biogeochemistry and alternate soil C and N
1091 models on C dynamics of CLM4, *Biogeosciences*, 10, 7109, 2013.

1092 Lawrence, D. M., Fisher, R. A., Koven, C. D., Oleson, K. W., Swenson, S. C., Bonan, G.,
1093 Collier, N., Ghimire, B., van Kampenhout, L., and Kennedy, D.: The Community Land Model
1094 version 5: Description of new features, benchmarking, and impact of forcing uncertainty, *Journal*
1095 *of Advances in Modeling Earth Systems*, 2019.

1096 Le Quéré, C., Andrew, R., Canadell, J. G., Sitch, S., Korsbakken, J. I., Peters, G. P., Manning, A.
1097 C., Boden, T. A., Tans, P. P., and Houghton, R. A.: Global carbon budget 2016, 2016.

1098 Le Quéré, C., Andrew, R. M., Friedlingstein, P., Sitch, S., Hauck, J., Pongratz, J., Pickers, P. A.,
1099 Korsbakken, J. I., Peters, G. P., and Canadell, J. G.: Global carbon budget 2018, *Earth System*
1100 *Science Data*, 10, 2141-2194, 2018.

1101 LeBauer, D. S. and Treseder, K. K.: Nitrogen limitation of net primary productivity in terrestrial
1102 ecosystems is globally distributed, *Ecology*, 89, 371-379, 2008.

1103 Lin, B.-L., Sakoda, A., Shibasaki, R., Goto, N., and Suzuki, M.: Modelling a global
1104 biogeochemical nitrogen cycle in terrestrial ecosystems, *Ecological Modelling*, 135, 89-110,
1105 2000.

1106 Luo, Y., Randerson, J. T., Friedlingstein, P., Hibbard, K., Hoffman, F., Huntzinger, D., Jones, C.,
1107 Koven, C., Lawrence, D., and Li, D.: A framework for benchmarking land models, 2012.

1108 Mao, J., Ricciuto, D. M., Thornton, P. E., Warren, J. M., King, A. W., Shi, X., Iversen, C. M.,
1109 and Norby, R. J.: Evaluating the Community Land Model in a pine stand with shading
1110 manipulations and $^{13}\text{CO}_2$ labeling, *Biogeosciences (Online)*, 13, 2016.

1111 Marklein, A. R. and Houlton, B. Z.: Nitrogen inputs accelerate phosphorus cycling rates across a
1112 wide variety of terrestrial ecosystems, *New Phytologist*, 193, 696-704, 2012.

1113 Matthews, E.: Global litter production, pools, and turnover times: Estimates from measurement
1114 data and regression models, *Journal of Geophysical Research: Atmospheres*, 102, 18771-18800,
1115 1997.

1116 McGill, W. and Cole, C.: Comparative aspects of cycling of organic C, N, S and P through soil
1117 organic matter, *Geoderma*, 26, 267-286, 1981.

1118 Melillo, J., Steudler, P., Aber, J., Newkirk, K., Lux, H., Bowles, F., Catricala, C., Magill, A.,
1119 Ahrens, T., and Morrisseau, S.: Soil warming and carbon-cycle feedbacks to the climate system,
1120 *Science*, 298, 2173-2176, 2002.

1121 Metcalfe, D. B., Ricciuto, D., Palmroth, S., Campbell, C., Hurry, V., Mao, J., Keel, S. G., Linder,
1122 S., Shi, X., and Näsholm, T.: Informing climate models with rapid chamber measurements of
1123 forest carbon uptake, *Global change biology*, 23, 2130-2139, 2017.

1124 Mitchard, E. T., Feldpausch, T. R., Brienen, R. J., Lopez-Gonzalez, G., Monteagudo, A., Baker,
1125 T. R., Lewis, S. L., Lloyd, J., Quesada, C. A., and Gloor, M.: Markedly divergent estimates of A
1126 mazon forest carbon density from ground plots and satellites, *Global Ecology and Biogeography*,
1127 23, 935-946, 2014.

1128 Nakhavali, M., Mercado, L. M., Hartley, I. P., Sitch, S., Cunha, F. V., di Ponzio, R., Lugli, L. F.,
1129 Quesada, C. A., Andersen, K. M., and Chadburn, S. E.: Representation of phosphorus cycle in
1130 Joint UK Land Environment Simulator (vn5. 5_JULES-CNP), *Geoscientific Model*
1131 *Development Discussions*, 1-24, 2021.

1132 Nasto, M. K., Alvarez-Clare, S., Lekberg, Y., Sullivan, B. W., Townsend, A. R., and Cleveland,
1133 C. C.: Interactions among nitrogen fixation and soil phosphorus acquisition strategies in lowland
1134 tropical rain forests, *Ecology Letters*, 17, 1282-1289, 2014.

1135 Norby, R. J., Gu, L., Haworth, I. C., Jensen, A. M., Turner, B. L., Walker, A. P., Warren, J. M.,
1136 Weston, D. J., Xu, C., and Winter, K.: Informing models through empirical relationships
1137 between foliar phosphorus, nitrogen and photosynthesis across diverse woody species in tropical
1138 forests of Panama, *New Phytologist*, 215, 1425-1437, 2017.

1139 Olander, L. P. and Vitousek, P. M.: Regulation of soil phosphatase and chitinase activity by N
1140 and P availability, *Biogeochemistry*, 49, 175-191, 2000.

1141 Oleson, K., Lawrence, D., Bonan, G., Drewniak, B., Huang, M., Koven, C., Levis, S., Li, F.,
 1142 Riley, W., and Subin, Z.: Technical Description of version 4.5 of the Community Land Model
 1143 (CLM)(NCAR Technical Note No. NCAR/TN-503+ STR). Citeseer, National Center for
 1144 Atmospheric Research, PO Box, 3000, 2013.
 1145 Pan, Y., Birdsey, R. A., Fang, J., Houghton, R., Kauppi, P. E., Kurz, W. A., Phillips, O. L.,
 1146 Shvidenko, A., Lewis, S. L., and Canadell, J. G.: A large and persistent carbon sink in the
 1147 world, *Science*, 333, 988-993, 2011.
 1148 Post, W. M., Pastor, J., Zinke, P. J., and Stangenberger, A. G.: Global patterns of soil nitrogen
 1149 storage, *Nature*, 317, 613-616, 1985.
 1150 Raczka, B., Duarte, H. F., Koven, C. D., Ricciuto, D., Thornton, P. E., Lin, J. C., and Bowling,
 1151 D. R.: An observational constraint on stomatal function in forests: evaluating coupled carbon and
 1152 water vapor exchange with carbon isotopes in the Community Land Model (CLM4. 5),
 1153 *Biogeosciences*, 13, 5183-5204, 2016.
 1154 Reed, S. C., Cleveland, C. C., and Townsend, A. R.: Relationships among phosphorus,
 1155 molybdenum and free-living nitrogen fixation in tropical rain forests: results from observational
 1156 and experimental analyses, *Biogeochemistry*, 1-13, 2013.
 1157 Reed, S. C., Yang, X., and Thornton, P. E.: Incorporating phosphorus cycling into global
 1158 modeling efforts: a worthwhile, tractable endeavor, *New Phytologist*, 208, 324-329, 2015.
 1159 Santoro, M., Beaudoin, A., Beer, C., Cartus, O., Fransson, J. E., Hall, R. J., Pathe, C.,
 1160 Schmullius, C., Schepaschenko, D., and Shvidenko, A.: Forest growing stock volume of the
 1161 northern hemisphere: Spatially explicit estimates for 2010 derived from Envisat ASAR, *Remote
 1162 Sensing of Environment*, 168, 316-334, 2015.
 1163 Sellar, A. A., Jones, C. G., Mulcahy, J., Tang, Y., Yool, A., Wiltshire, A., O'connor, F. M.,
 1164 Stringer, M., Hill, R., and Palmieri, J.: UKESM1: Description and evaluation of the UK Earth
 1165 System Model, *Journal of Advances in Modeling Earth Systems*, 2019.
 1166 Shabanov, N. V., Huang, D., Yang, W., Tan, B., Knyazikhin, Y., Myneni, R. B., Ahl, D. E.,
 1167 Gower, S. T., Huete, A. R., and Aragão, L. E. O.: Analysis and optimization of the MODIS leaf
 1168 area index algorithm retrievals over broadleaf forests, *IEEE Transactions on Geoscience and
 1169 Remote Sensing*, 43, 1855-1865, 2005.
 1170 Smil, V.: P HOSPHORUS IN THE E NVIRONMENT: Natural Flows and Human Interferences,
 1171 *Annual review of energy and the environment*, 25, 53-88, 2000.
 1172 Smith, B., Warlind, D., Arneeth, A., Hickler, T., Leadley, P., Siltberg, J., and Zaehle, S.:
 1173 Implications of incorporating N cycling and N limitations on primary production in an
 1174 individual-based dynamic vegetation model, *Biogeosciences*, 11, 2027-2054, 2014.
 1175 Sun, Y., Goll, D. S., Ciais, P., Peng, S., Margalef, O., Asensio, D., Sardans, J., and Peñuelas, J.:
 1176 Spatial pattern and environmental drivers of acid phosphatase activity in Europe, 2020.
 1177 Sun, Y., Goll, D. S., Chang, J., Ciais, P., Guenet, B., Helfenstein, J., Huang, Y., Lauerwald, R.,
 1178 Maignan, F., and Naipal, V.: Global evaluation of the nutrient-enabled version of the land
 1179 surface model ORCHIDEE-CNP v1. 2 (r5986), *Geoscientific Model Development*, 14, 1987-
 1180 2010, 2021.
 1181 Sun, Y., Peng, S., Goll, D. S., Ciais, P., Guenet, B., Guimberteau, M., Hinsinger, P., Janssens, I.
 1182 A., Peñuelas, J., and Piao, S.: Diagnosing phosphorus limitations in natural terrestrial ecosystems
 1183 in carbon cycle models, *Earth's future*, 5, 730-749, 2017.
 1184 Terrer, C., Jackson, R. B., Prentice, I. C., Keenan, T. F., Kaiser, C., Vicca, S., Fisher, J. B.,
 1185 Reich, P. B., Stocker, B. D., and Hungate, B. A.: Nitrogen and phosphorus constrain the CO₂
 1186 fertilization of global plant biomass, *Nature Climate Change*, 9, 684-689, 2019.

1187 Thornton, P., Doney, S., Lindsay, K., Moore, J., Mahowald, N., Randerson, J., Fung, I.,
 1188 Lamarque, J., Feddesma, J., and Lee, Y.: Carbon-nitrogen interactions regulate climate-carbon
 1189 cycle feedbacks: results from an atmosphere-ocean general circulation model, 2009.
 1190 Thornton, P. E., Lamarque, J.-F., Rosenbloom, N. A., and Mahowald, N. M.: Influence of
 1191 carbon-nitrogen cycle coupling on land model response to CO₂ fertilization and climate
 1192 variability, *Global Biogeochemical Cycles*, 21, GB4018, 10.1029/2006gb002868, 2007.
 1193 Thum, T., Caldararu, S., Engel, J., Kern, M., Pallandt, M., Schnur, R., Yu, L., and Zaehle, S.: A
 1194 new terrestrial biosphere model with coupled carbon, nitrogen, and phosphorus cycles (QUINCY
 1195 v1. 0; revision 1772), *Geoscientific Model Development*, 12, 4781-4802, 2019.
 1196 Todd-Brown, K., Randerson, J., Post, W., Hoffman, F., Tarnocai, C., Schuur, E., and Allison, S.:
 1197 Causes of variation in soil carbon simulations from CMIP5 Earth system models and comparison
 1198 with observations, *Biogeosciences*, 10, 1717-1736, 2013.
 1199 Treseder, K. K. and Vitousek, P. M.: Effects of soil nutrient availability on investment in
 1200 acquisition of N and P in Hawaiian rain forests, *Ecology*, 82, 946-954, 2001.
 1201 Van den Hurk, B., Kim, H., Krinner, G., Seneviratne, S. I., Derksen, C., Oki, T., Douville, H.,
 1202 Colin, J., Ducharne, A., and Cheruy, F.: LS3MIP (v1. 0) contribution to CMIP6: the Land
 1203 Surface, Snow and Soil moisture Model Intercomparison Project-aims, setup and expected
 1204 outcome, *Geoscientific Model Development*, 9, 2809-2832, 2016.
 1205 Vicca, S., Luysaert, S., Penuelas, J., Campioli, M., Chapin III, F., Ciais, P., Heinemeyer, A.,
 1206 Högberg, P., Kutsch, W., and Law, B. E.: Fertile forests produce biomass more efficiently,
 1207 *Ecology letters*, 15, 520-526, 2012.
 1208 Vitousek, P. M., Menge, D. N., Reed, S. C., and Cleveland, C. C.: Biological nitrogen fixation:
 1209 rates, patterns and ecological controls in terrestrial ecosystems, *Philosophical Transactions of the*
 1210 *Royal Society B: Biological Sciences*, 368, 20130119, 2013.
 1211 Vitousek, P. M., Porder, S., Houlton, B. Z., and Chadwick, O. A.: Terrestrial phosphorus
 1212 limitation: mechanisms, implications, and nitrogen-phosphorus interactions, *Ecological*
 1213 *applications*, 20, 5-15, 2010.
 1214 Walker, A. P., Beckerman, A. P., Gu, L., Kattge, J., Cernusak, L. A., Domingues, T. F., Scales,
 1215 J. C., Wohlfahrt, G., Wullschleger, S. D., and Woodward, F. I.: The relationship of leaf
 1216 photosynthetic traits—V_{cmax} and J_{max}—to leaf nitrogen, leaf phosphorus, and specific leaf area: a
 1217 meta-analysis and modeling study, *Ecology and evolution*, 4, 3218-3235, 2014.
 1218 Walker, T. and Syers, J.: The fate of phosphorus during pedogenesis, *Geoderma*, 15, 1-19, 1976.
 1219 Wang, Y., Ciais, P., Goll, D. S., Huang, Y., Luo, Y., Wang, Y.-P., Bloom, A. A., Broquet, G.,
 1220 Hartmann, J., and Peng, S.: GOLUM-CNP v1. 0: a data-driven modeling of carbon, nitrogen and
 1221 phosphorus cycles in major terrestrial biomes, 2018.
 1222 Wang, Y.-P., Law, R. M., and Pak, B.: A global model of carbon, nitrogen and phosphorus
 1223 cycles for the terrestrial biosphere, *Biogeosciences*, 7, 2261-2282, 10.5194/bg-7-2261-2010,
 1224 2010.
 1225 Wang, Y. P., Houlton, B. Z., and Field, C. B.: A model of biogeochemical cycles of carbon,
 1226 nitrogen, and phosphorus including symbiotic nitrogen fixation and phosphatase production,
 1227 *Global Biogeochemical Cycles*, 21, GB1018, 10.1029/2006gb002797, 2007.
 1228 Welp, L. R., Keeling, R. F., Meijer, H. A., Bollenbacher, A. F., Piper, S. C., Yoshimura, K.,
 1229 Francey, R. J., Allison, C. E., and Wahlen, M.: Interannual variability in the oxygen isotopes of
 1230 atmospheric CO₂ driven by El Niño, *Nature*, 477, 579-582, 2011.

1231 Wieder, W. R., Cleveland, C. C., Lawrence, D. M., and Bonan, G. B.: Effects of model structural
1232 uncertainty on carbon cycle projections: biological nitrogen fixation as a case study,
1233 Environmental Research Letters, 10, 044016, 2015a.

1234 Wieder, W. R., Cleveland, C. C., Smith, W. K., and Todd-Brown, K.: Future productivity and
1235 carbon storage limited by terrestrial nutrient availability, Nature Geoscience, 8, 441, 2015b.

1236 Wieder, W. R., Lawrence, D. M., Fisher, R. A., Bonan, G. B., Cheng, S. J., Goodale, C. L.,
1237 Grandy, A. S., Koven, C. D., Lombardozzi, D. L., and Oleson, K. W.: Beyond static
1238 benchmarking: Using experimental manipulations to evaluate land model assumptions, Global
1239 Biogeochemical Cycles, 33, 1289-1309, 2019.

1240 Wright, S. J., Turner, B. L., Yavitt, J. B., Harms, K. E., Kaspari, M., Tanner, E. V., Bujan, J.,
1241 Griffin, E. A., Mayor, J. R., and Pasquini, S. C.: Plant responses to fertilization experiments in
1242 lowland, species-rich, tropical forests, Ecology, 99, 1129-1138, 2018.

1243 Xu, R. I. and Prentice, I. C.: Terrestrial nitrogen cycle simulation with a dynamic global
1244 vegetation model, Global Change Biology, 14, 1745-1764, 10.1111/j.1365-2486.2008.01625.x,
1245 2008.

1246 Yang, X. and Post, W.: Phosphorus transformations as a function of pedogenesis: a synthesis of
1247 soil phosphorus data using Hedley fractionation method, Biogeosciences, 8, 2907-2916, 2011.

1248 Yang, X., Post, W., Thornton, P., and Jain, A.: The distribution of soil phosphorus for global
1249 biogeochemical modeling, Biogeosciences, 10, 2525-2537, 2013.

1250 Yang, X., Thornton, P., Ricciuto, D., and Post, W.: The role of phosphorus dynamics in tropical
1251 forests—a modeling study using CLM-CNP, Biogeosciences, 11, 1667-1681, 2014.

1252 Yang, X., Thornton, P. E., Ricciuto, D. M., and Hoffman, F. M.: Phosphorus feedbacks
1253 constraining tropical ecosystem responses to changes in atmospheric CO₂ and climate,
1254 Geophysical Research Letters, 43, 7205-7214, 10.1002/2016GL069241, 2016.

1255 Yang, X., Wittig, V., Jain, A., and Post, W.: Integration of nitrogen cycle dynamics into the
1256 Integrated Science Assessment Model for the study of terrestrial ecosystem responses to global
1257 change, Global Biogeochemical Cycles, 23, 2009.

1258 Yang, X., Ricciuto, D. M., Thornton, P. E., Shi, X., Xu, M., Hoffman, F., and Norby, R. J.: The
1259 effects of phosphorus cycle dynamics on carbon sources and sinks in the Amazon region: a
1260 modeling study using ELM v1, Journal of Geophysical Research: Biogeosciences, 2019.

1261 Zaehle, S., Friend, A., Friedlingstein, P., Dentener, F., Peylin, P., and Schulz, M.: Carbon and
1262 nitrogen cycle dynamics in the O-CN land surface model: 2. Role of the nitrogen cycle in the
1263 historical terrestrial carbon balance, Global Biogeochemical Cycles, 24, 2010.

1264 Zhang, Q., Wang, Y.-P., Matear, R., Pitman, A., and Dai, Y.: Nitrogen and phosphorus
1265 limitations significantly reduce future allowable CO₂ emissions, Geophysical Research Letters,
1266 41, 632-637, 2014.

1267 Zhu, Q., Riley, W. J., Tang, J., Collier, N., Hoffman, F. M., Yang, X., and Bisht, G.:
1268 Representing nitrogen, phosphorus, and carbon interactions in the E3SM land model:
1269 Development and global benchmarking, Journal of Advances in Modeling Earth Systems, 11,
1270 2238-2258, 2019.

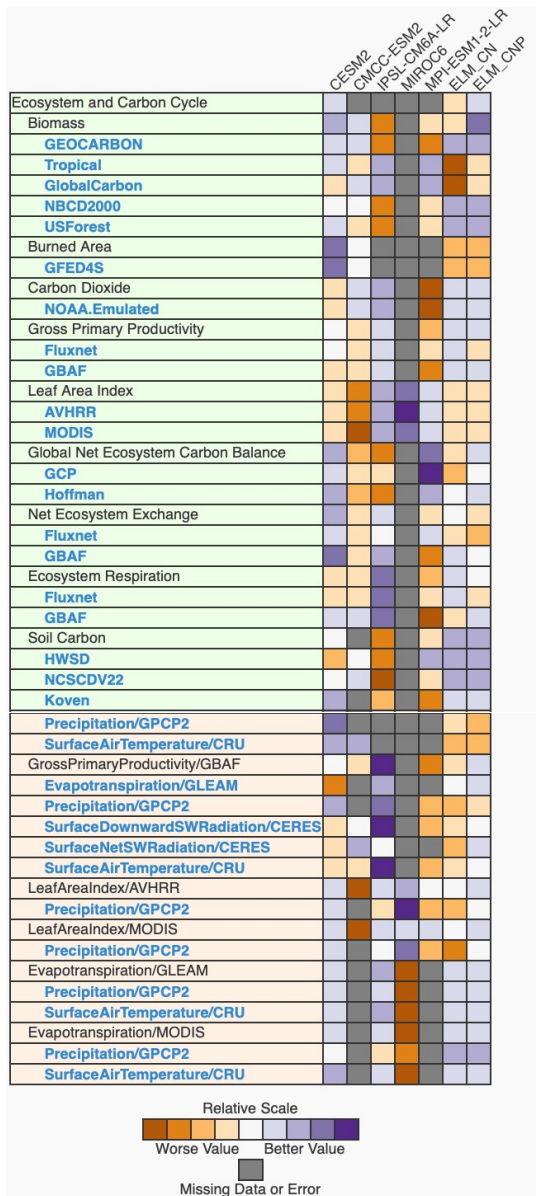
1271

1272

1273

1274

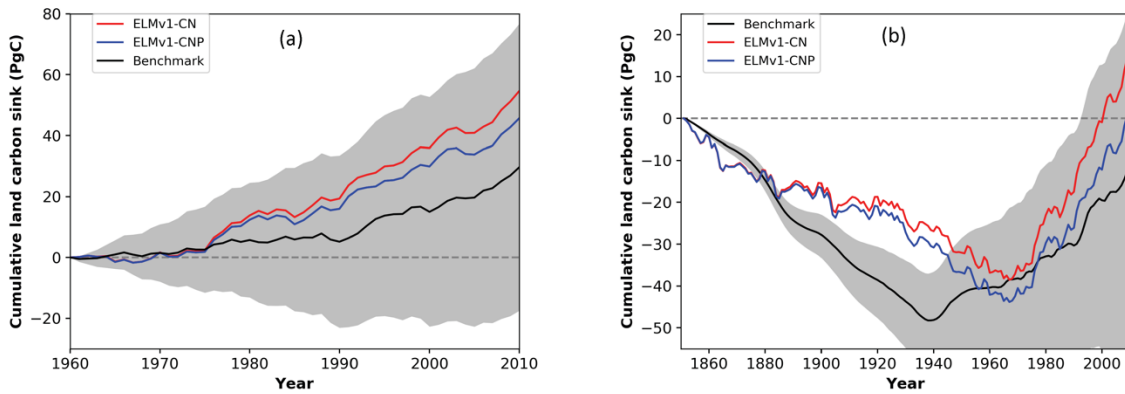
1275
1276
1277
1278
1279
1280
1281
1282
1283
1284
1285
1286
1287



1288
 1289
 1290
 1291
 1292
 1293
 1294
 1295
 1296

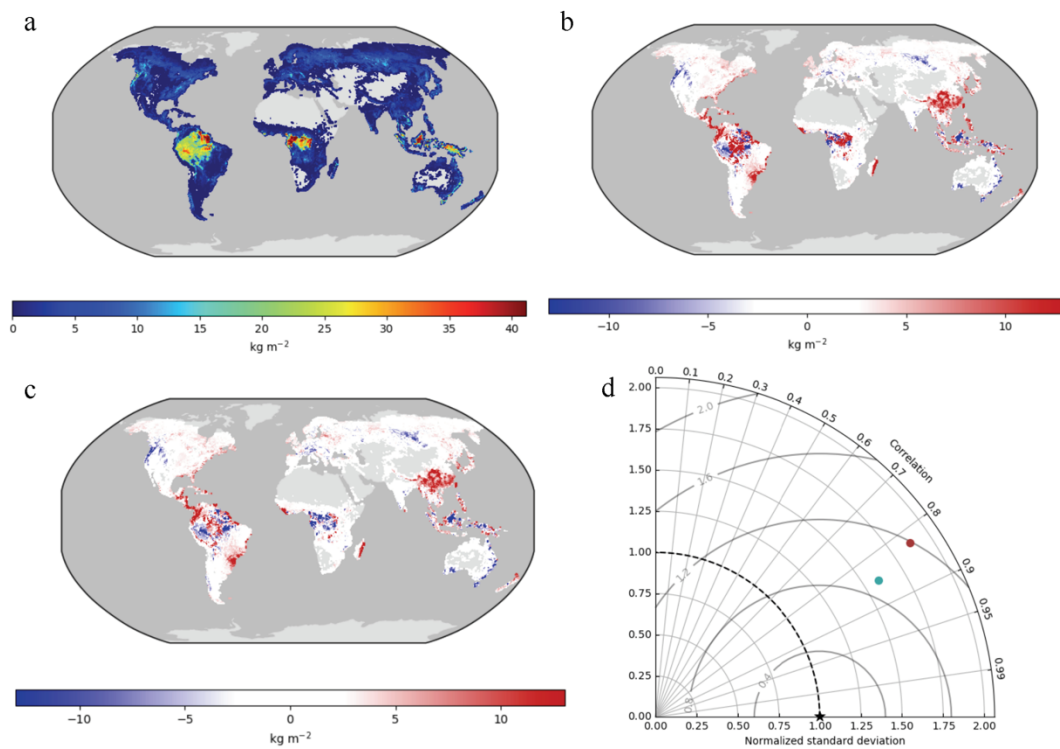
Figure 1: ILAMB carbon cycle scores for ELMv1-CNP and ELM-CN and a few land models in CMIP6. Shown here is the relative score, indicating the performance of each model relative to other models. References for benchmarking data for each variable are provided in Table S4. The datasets that are in green boxes are either carbon pools or fluxes while the datasets in orange boxes are relationships between carbon pools/fluxes and environmental variables such as precipitation or temperature. Outputs for other land models are from the LS3MIP offline simulations archive in CMIP6. These simulations were performed using the same resolution and forcing data as this study. CLM4.5 is the land model in CMCC-ESM2. CLM5 is the land model for

1297 CESM2. OCHIDEE is the land model for IPSL. JSBACH is the land model for MPI-ESM1.2. VISIT is
1298 the land model for MIROC6.



1299
1300 Figure 2: ELMv1-CNP and ELMv1-CN simulated global land carbon accumulation for the time
1301 period (a) 1960-2010 and (b) and 1850-2010. Benchmark data (black lines with uncertainty
1302 estimate in grey) are from (a) Global carbon project (Le Quere et al., 2016) and (b) Hoffman et
1303 al. (2014).

1304
1305
1306



1307

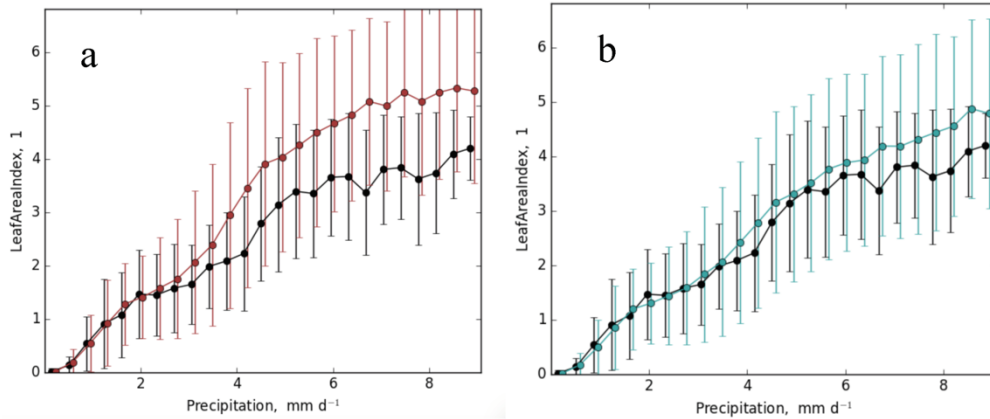
1308

1309

1310 Figure 3: Global pattern of simulated biomass: (a) benchmark data, (b) ELMv1-CN bias (c)
 1311 ELMv1-CNP bias and (d) spatial Taylor diagram for model-benchmark comparison (red dot is for
 1312 ELMv1-CN and blue dot is for ELMv1-CNP). Benchmark data here is from the GEOCARBON
 1313 product (Saatchi et al.,2011).

1314

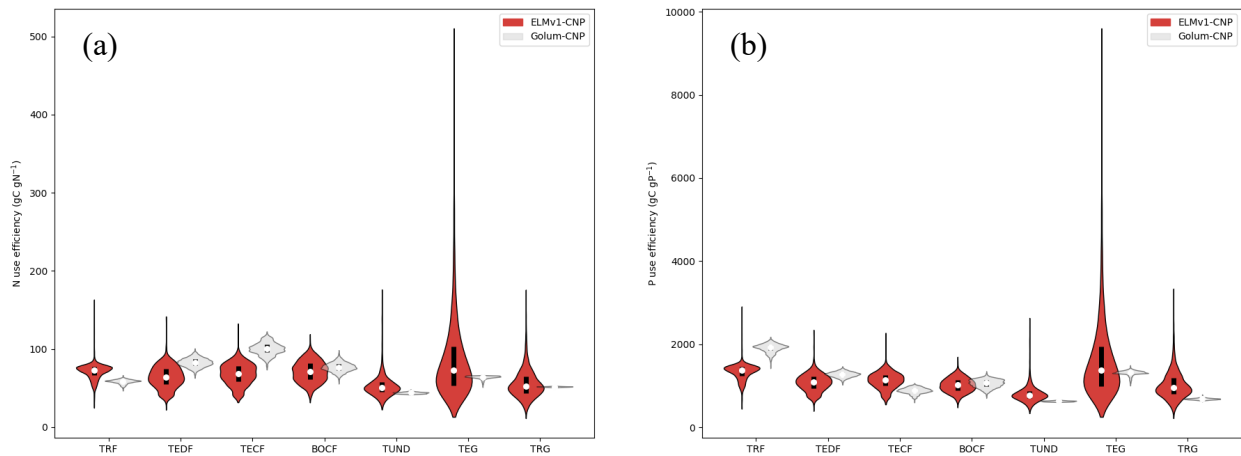
1315



1316
1317

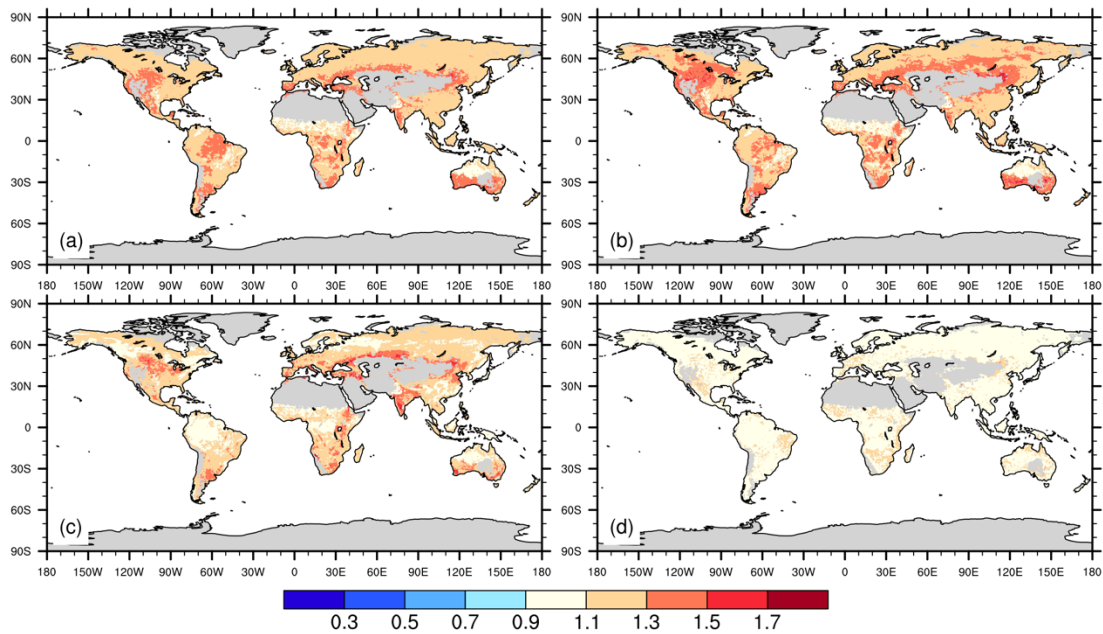
1318 Figure 4: ILAMB relationship plot between LAI and climatological annual precipitation and (a)
1319 ELMv1-CN (b) ELMv1-CNP. Black line is the observationally derived relationship. Error bars
1320 indicate one standard deviation of LAI for all grid cells within the precipitation bin. Observed
1321 LAI is from MODIS LAI product.

1322
1323
1324
1325
1326
1327
1328
1329



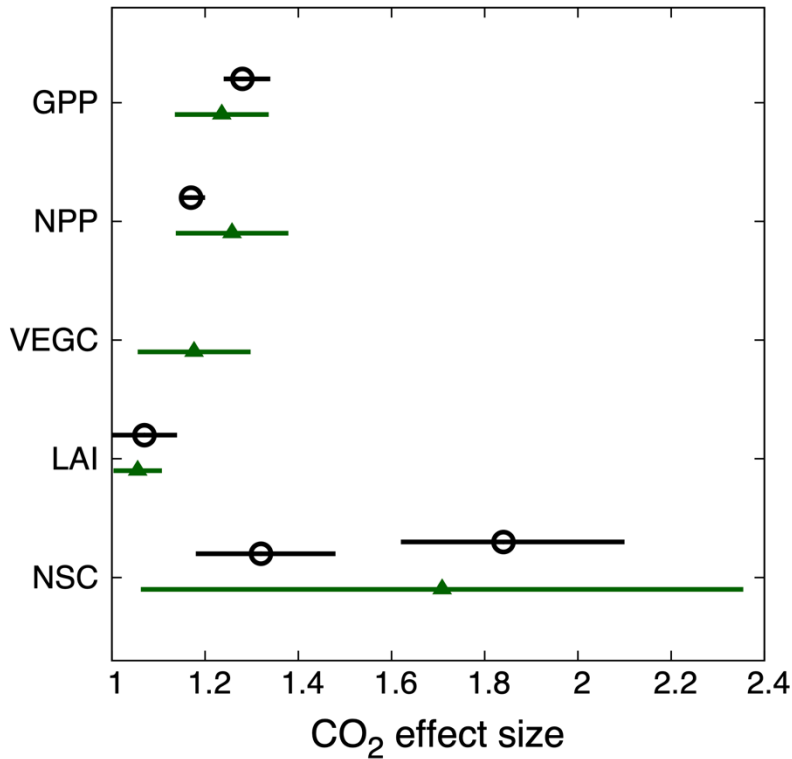
1330
 1331
 1332
 1333
 1334
 1335
 1336
 1337
 1338
 1339
 1340

Figure 5: Violin plots of (a) nitrogen use efficiency (NUE) and (b) phosphorus use efficiency (PUE) from ELMv1-CNP and GOLUM-CNP for seven biomes: tropical rainforest (TRF), temperate deciduous forest (TEDF), temperate coniferous forest (TECF), boreal coniferous forest (BOCF), temperate grassland (TEG) and tropical grassland (TRG). Plots show the medians of all grid cells in each biome (open circles) and the probability density distribution (balloons).



1341
 1342
 1343
 1344
 1345
 1346
 1347

Figure 6: Spatial distribution of the effect size of CO₂ enrichment on (a) GPP (b) NPP (c) Vegetation carbon (d) LAI. Effect sizes were calculated for each grid cell as the mean annual values of GPP, NPP, vegetation carbon and LAI from CO₂ enrichment simulation divided those from the control simulations between 2001-2010.

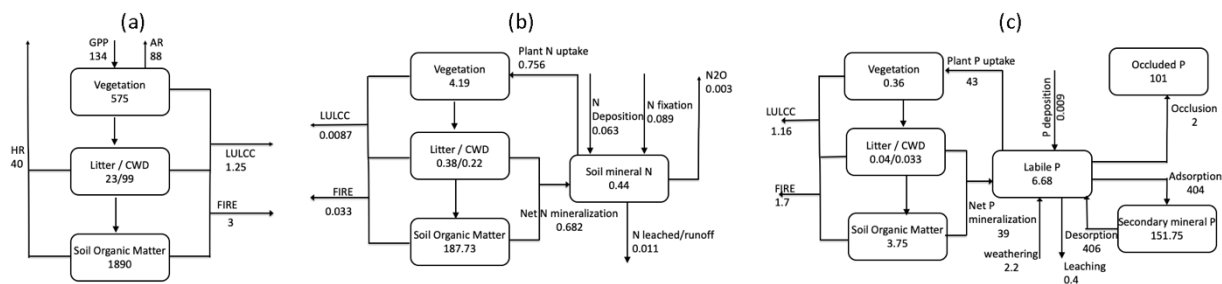


1348

1349 Figure 7: Observed (open circles) and simulated (green triangles) effect size of CO₂ enrichment
 1350 on GPP, NPP, LAI, vegetation carbon and non-structural carbon. Observations show the mean
 1351 (±95% confidence interval; Ainsworth and Long, 2005). There are two observations of NSC
 1352 shown here, one is for sugar with a mean value of 1.3 and the other is for starch with a mean
 1353 value of 1.8, while model conceptualization of NSC includes both sugar and starch. Simulated
 1354 responses show the global mean effect sizes (± stand derivation; calculated to provide an
 1355 estimate of spatial variation).

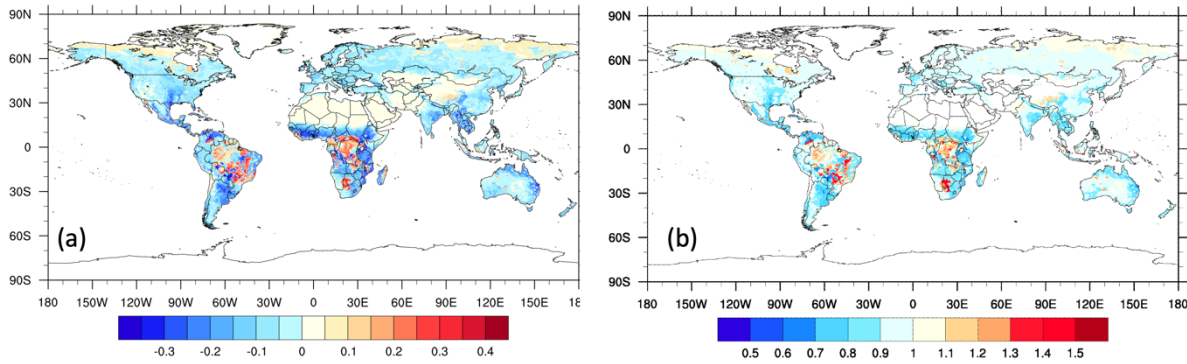
1356

1357



1358
 1359
 1360 Figure 8: (left) terrestrial C cycle, (middle) N cycle, and (right) P cycle as simulated by ELMv1-
 1361 CNP, shown here are mean values between 2001-2010. Vegetation and soil C, N and P pools
 1362 are in units of Pg C, Pg N and Pg P, respectively. C and N fluxes are given in Pg C yr⁻¹ and Pg N yr⁻¹,
 1363 and P fluxes are given in Tg P yr⁻¹. AR stands for autotrophic respiration and HR stands for
 1364 heterotrophic respiration.

1365
 1366
 1367
 1368
 1369
 1370
 1371
 1372
 1373
 1374
 1375



1376

1377 Figure 9: (a) Spatial variation of the extent of nutrient limitation on plant growth. Regions with
 1378 a negative value are more limited by N, while regions with a positive value are more limited by
 1379 P. Larger absolute values are associated with stronger limitation. Values plotted are the
 1380 proportion by which plant growth is reduced due to N limitation or P limitation: $1-f_P$ when f_P
 1381 $< f_N$ and f_N-1 when $f_N < f_P$, where f_P is the limitation factor on plant growth considering P
 1382 supply and demand, while f_N is the limitation factor on plant growth considering N supply and
 1383 demand (Yang *et al.*, 2014). (b) Spatial variation of the ratios between P limitation and N
 1384 limitation indicating the degree of co-limitation. Values plotted are the ratios between f_N and
 1385 f_P : f_N/f_P . Regions with values less than 1 indicate more N limitation and regions with values
 1386 greater than 1 are more limited by P. Values close to 1 indicate NP co-limitation. Definition of
 1387 colimitation is subjective here, but difference of 10% or less between the values for f_N and f_P
 1388 would lead to a range of about 0.9 to 1.1 in the plotted ratio.

1389

1390

1391

1392

1393

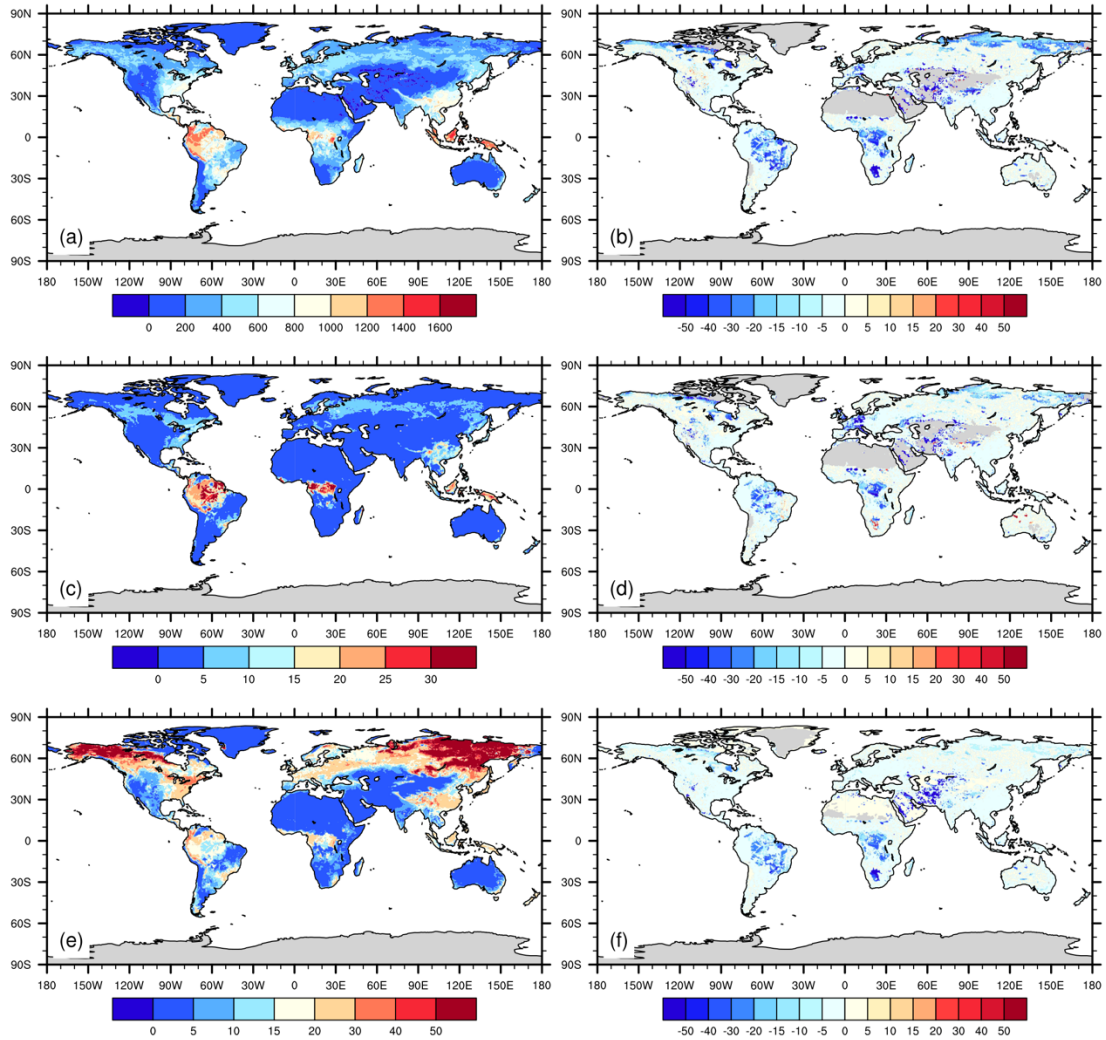
1394

1395

1396

1397

1398



1400

1401

1402 Fig. 10: Average estimates of (a) net primary productivity ($\text{g C m}^{-2} \text{ yr}^{-1}$) (c) vegetation carbon (kg C m^{-2}) and (e) soil organic carbon (kg C m^{-2}) for the years 2001-2010 and the effects of

1403 phosphorus dynamics (expressed as percentage deviation between CNP and CN configurations,

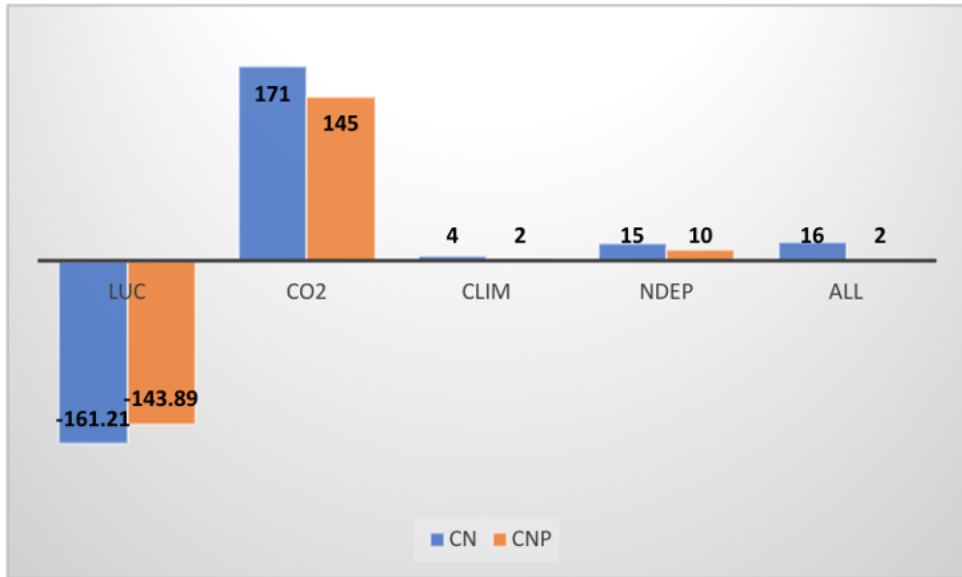
1404 unitless) on (b) net primary productivity (d) vegetation carbon (f) soil carbon as estimated by

1405 ELMv1.

1406

1407

1408



1409

1410 Fig. 11: Cumulative global carbon storage (Pg C) from 1850 to 2010 from ELMv1-CN and ELMv1-
 1411 CNP simulations with changes in land use and land cover change (LUC), atmospheric CO₂ (CO₂),
 1412 climate (CLIM), N deposition (NDEP), and all factor combined (ALL). These are calculated as the
 1413 accumulation of NEE between 1850 and 2010 for the historical transient model simulations
 1414 listed in Table 1.

1415

1416

1417

1418

1419

1420

1421

1422

1423

1424

1425

1426

1427

1428

1429
1430
1431

Table 1: Summary of model simulations

Experiment	P coupling	CO ₂ forcing	LULCC	Climate forcing	N depos
Ctrl_CN	off	1850	1850	steady state ^a	1850
Ctrl_CNP	on	1850	1850	steady state ^a	1850
Hist_CN_CO ₂	off	transient	1850	steady state ^a	1850
Hist_CNP_CO ₂	on	transient	1850	steady state ^a	1850
Hist_CN_LUC	off	1850	transient	steady state ^a	1850
Hist_CNP_LUC	on	1850	transient	steady state ^a	1850
Hist_CN_climate	off	1850	1850	transient ^b	1850
Hist_CNP_climate	on	1850	1850	transient ^b	1850
Hist_CN_NDep	off	1850	1850	steady state ^a	transient
Hist_CNP_Ndep	on	1850	1850	steady state ^a	transient
Hist_CN_all	off	Transient	A d	transient ^b	transient
Hist_CNP_all	on	transient	transient	transient ^b	transient
FACE_CO ₂	on	+200ppm (1991-2010)	transient	transient ^b	transient

1432 a Cycling of 20-year time series of GSWP3 reanalysis product (1901-1920)

1433 b Historical time series of GSWP3 reanalysis product (1901-2010)

1434
1435

1436

1437

1438

1439

1440

1441

1442

1443

1444

1445

1446

1447

1448

1449 Table 2: Comparison of ELMv1-CNP Simulated Mean Global Stocks and Fluxes of C, N and P
 1450 between 2001 and 2010 to Observation-based Estimates

	ELMv1-CNP	Observation-based Estimates		
			Source	Methodology
GPP (Pg C yr ⁻¹)	134.15	123±8	Beer et al., 2010	Using eddy covariance flux data and various diagnostic models
		150-175	Welp et al., 2011	Based on oxygen isotopes of atmospheric CO ₂
		119±6	Jung et al., 2011	upscaled FLUXNET observations to the global scale using the machine learning technique, model tree ensembles (MTE).
		121.60 - 129.42	Zhang et al., 2017	Light use efficiency theory, MODIS satellite data and climate data
		140	Joiner et al., 2018	Satellite Data-Driven Models and Eddy Covariance Flux Data
NPP (Pg C yr ⁻¹)	46.09	55±11	Turner et al., 2006	MODIS products
		33-49	Smith et al., 2016	MODIS NPP algorithm driven by long-term Global Inventory Modeling and Mapping Studies (GIMMS) FPAR and LAI data
Vegetation C (Pg C)	575.45	550±100	Houghton, 2003	Literature synthesis
		560±94	Defries et al., 1999	
Soil carbon (Pg C)	1890.78	1750±250	Houghton, 2003	Literature synthesis
		2344	Jobbagy and Jackson, 2000	based on >2700 soil profiles in three global databases supplemented with data for climate, vegetation, and land use.
		3000	Kochy et al., 2015	Based on the Harmonized World Soil Database(HWSD), but with more detailed estimates for permafrost and tropical wetland soil carbon
		2376–2456	Batjes, 2014	Top 2m. Based on 4353 soil profiles distributed globally and the FAO Soil Map of the World.
Top 1m soil carbon (Pg C)	1134.41	1462-1548	Batjes, 2014	Based on 4353 soil profiles distributed globally and the FAO Soil Map of the World.
		1325	Kochy et al., 2015	Based on the Harmonized World Soil Database(HWSD), but with more detailed estimates for permafrost and tropical wetland soil carbon
		1502	Jobbagy and Jackson, 2000	based on >2700 soil profiles in three global databases supplemented with

				data for climate, vegetation, and land use.
Soil organic N (Pg N)	188.79	95	Post et al. 1985	Based on 3100 soil profiles and a global map of Holdridge life zones
		133-140	Batjes et al., 2014	Top 1m. Based on 4353 soil profiles distributed globally and the FAO Soil Map of the World
N fixation (Tg N yr ⁻¹)	89	40-100	Vitousek et al., 2013	Estimates for Pre-industrial. Combining information on N fluxes with ¹⁵ N relative abundance data for terrestrial ecosystems
		52-130	Davies-Barnard and Friedlingstein (2020)	Based on a comprehensive meta-analysis of field measurements
N uptake (Tg N yr ⁻¹)	760	570	Wang et al., 2018	Data-driven estimates. Observations include observed stoichiometric ratios, N and P external input fluxes, and the fraction of gaseous losses of N to total (gaseous and leaching) losses of N from a global data set of ¹⁵ N measurements in soils
N Leaching (Tg N yr ⁻¹)	12	38	Wang et al., 2018	Data-driven estimates. See above
		28	Mayorga et al., 2010	based on a mass-balance approach for the land surface (watershed) and river system for year 2000
P uptake (Tg P yr ⁻¹)	43	26	Wang et al., 2018	Data-driven estimates. See above
P leaching (Tg P yr ⁻¹)	0.46	2.6	Wang et al., 2018	Data-driven estimates. See above
P occlusion (Tg P yr ⁻¹)	1.85	1.3	Wang et al., 2018	Data-driven estimates. See above

1451
1452
1453
1454
1455
1456
1457
1458
1459
1460
1461
1462
1463
1464
1465